การเตรียมตะแกรงร่อนโมเลกุลซีโอไลต์สำหรับแยกน้ำออกจากสารละลายเอทานอล

นายก้องหล้า หมื่นภูวงค์

วิทยานิพนธ์นี้เป็นส่วนหนึ่งของการศึกษาตามหลักสูตรปริญญาวิทยาศาสตรมหาบัณฑิต

สาขาวิชาเคมี

มหาวิทยาลัยเทคโนโลยีสุรนารี

ปีการศึกษา 2554

PREPARATION OF ZEOLITE MOLECULAR

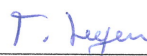# SIEVES FOR WATER SEPARATION FROM

ETHANOL SOLUTION

Kongla Muenpoowonk

A Thesis Submitted in Partial Fulfillment of the Requirements for the

Degree of Master of Science in Chemistry

Suranaree University of Technology

Academic Year 2011

PREPARATION OF ZEOLITE MOLECULAR SIEVES FOR

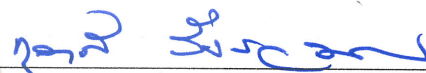# WATER SEPARATION FROM ETHANOL SOLUTION

Suranaree University of Technology has approved this thesis submitted in partial fulfillment of the requirements for a Master's Degree.

Thesis Examining Committee

_____

(Asst. Prof. Dr. Thanaporn Manyum)

Chairperson

_____

(Asst. Prof. Dr. Kunwadee Rangsriwatananon)

Member (Thesis Advisor)

_____

(Prof. Dr. Jatuporn Wittayakun)

Member

_____

(Asst. Prof. Dr. Sanchai Prayoonpokarach)

Member

_____
(Prof. Dr. Santi Maensiri)

Vice Rector for Academic Affairs

and Internationalization

_____
(Asst. Prof. Dr. Worawat Meevasana)

Dean of Institute of Science

ก้องหล้า หมื่นภูวงศ์ : การเตรียมตะแกรงร่อนโมเลกุลซีโอไลต์สำหรับแยกน้ำออกจาก
สารละลายเอทานอล (PREPARATION OF ZEOLITE MOLECULAR SIEVES FOR
WATER SEPARATION FROM ETHANOL SOLUTION) อาจารย์ที่ปรึกษา :
ผู้ช่วยศาสตราจารย์ ดร.กุลวดี รังษีวัฒนานนท์, 90 หน้า.

งานนี้มีวัตถุประสงค์เพื่อกำจัดน้ำออกจากสารละลายเอทานอล โดยใช้กระบวนการดูดซับ
ด้วยตะแกรงร่อนโมเลกุลซีโอไลต์ ได้ทำการสังเคราะห์ตะแกรงร่อนโมเลกุลซีโอไลต์ชนิดต่าง ๆ
และใช้เป็นตัวดูดซับน้ำ อะนาลซิมและแคนคริไนต์สังเคราะห์ได้จากไดอะตอไมต์ ส่วนซีโอไลต์
โซเดียมเอ (zeolite NaA) และซีโอไลต์โซเดียมเอ็กซ์ (zeolite NaX) สังเคราะห์ได้จากเกาลีน ซึ่ง
พบว่าผลิตภัณฑ์ที่ได้มีลักษณะเฉพาะของซีโอไลต์แต่ละชนิดโดยมีเพียงวัฏภาคเดียวและมีความเป็น
ผลึกสูง ซีโอไลต์โซเดียมเอและซีโอไลต์โซเดียมเอ็กซ์ที่ปรับเปลี่ยนด้วย K^+ Mg^{2+} Ca^{2+} Sr^{2+} Co^{2+}
Ni^{2+} Cu^{2+} และ Zn^{2+} หลังจากการปรับเปลี่ยนด้วยแคตไอออน พบว่าโครงสร้างของซีโอไลต์ถูก
ทำลายและร้อยละความเป็นผลึกลดลงร้อยละ 20 - 60 ขึ้นอยู่กับชนิดของซีโอไลต์และแคตไอออน

การศึกษาการดูดซับน้ำจากเอทานอลเข้มข้นร้อยละ 85.0 โดยปริมาตร โดยใช้ ซีโอไลต์
โซเดียมเอ ซีโอไลต์โซเดียมเอ็กซ์และซีโอไลต์โซเดียมเอ ซีโอไลต์โซเดียมเอ็กซ์ที่ถูกปรับเปลี่ยน
ด้วย K^+ Mg^{2+} Ca^{2+} Sr^{2+} Ni^{2+} Cu^{2+} และ Zn^{2+} พบว่าความเข้มข้นของเอทานอลเพิ่มขึ้นจากร้อยละ
85.0 โดยปริมาตร เป็นร้อยละ 86.5 - 93.1 โดยปริมาตร แต่พบว่าความเข้มข้นของเอทานอลเพิ่ม
สูงขึ้นถึงร้อยละ 98.2 โดยปริมาตร เมื่อซีโอไลต์โซเดียมเอ ซีโอไลต์โซเดียมเอ็กซ์ที่ถูกปรับเปลี่ยน
ด้วย Co^{2+} เมื่อใช้เอทานอลที่มีความเข้มข้นเริ่มต้นร้อยละ 95.0 โดยปริมาตร พบว่าสามารถเพิ่มความ
เข้มข้นของเอทานอลเป็นร้อยละ 99.1 - 99.8 โดยปริมาตร ในขณะที่ตัวดูดซับที่เหลือสามารถเพิ่ม
ความเข้มข้นของเอทานอลได้เพียงประมาณร้อยละ 1

ในกรณีของอะนาลซิมและแคนคริไนต์พบว่าความเข้มข้นของเอทานอลเพิ่มขึ้นจากร้อยละ
85.0 โดยปริมาตร เป็นร้อยละ 96.4 และ 94.9 โดยปริมาตร ตามลำดับ และเมื่อใช้ความเข้มข้นเริ่มต้น
เป็นร้อยละ 95.0 จะมีความเข้มข้นเของเอทานอลพิ่มจากร้อยละ 95.0 เป็นร้อยละ 99.3 และ 99.6 โดย
ปริมาตร ตามลำดับ

สาขาวิชาเคมี   ลายมือชื่อนักศึกษา_____
ปีการศึกษา 2554   ลายมือชื่ออาจารย์ที่ปรึกษา_____

KONGLA MUENPOOWONK : PREPARATION OF ZEOLITE MOLECULAR SIEVES FOR WATER SEPARATION FROM ETHANOL SOLUTION. THESIS ADVISOR : ASST. PROF. KUNWADEE RANGSRIWATANANON, Ph.D. 90 PP.

ZEOLITE/ANALCIME/CANCRINITE/MOLECULAR SIEVES/ETHANOL/ SEPARATION

The elimination of water from ethanol solution was an objective in this work and the adsorption process with zeolite molecular sieves was applied. Various zeolite molecular sieves were synthesized and were used to adsorb water. Analcime and cancrinite were successfully synthesized from diatomite; and zeolite NaA and NaX were from kaolin. All the products showed only single phase of each zeolite with high crystallinity. Only zeolite NaA and NaX were modified with the following cations namely K^+, Mg^{2+}, Ca^{2+}, Sr^{2+}, Co^{2+}, Ni^{2+} Cu^{2+}, and Zn^{2+}. After cationic modification it was found that the zeolite framework was destroyed and the percentage of crystallinity was decreased 20 - 60% depending on the type of zeolite and cation.

For the water adsorption from 85.0% v/v ethanol, it was found that the percentage of ethanol was increased from 85.0% up to 86.5 - 93.1% v/v with zeolite NaA, NaX and modified zeolite NaA and NaX with K^+, Mg^{2+}, Ca^{2+}, Sr^{2+}, Ni^{2+}, Cu^{2+}, and Zn^{2+}. However, the ethanol concentration was significantly increased to 98.2% v/v when using modified zeolite NaA and NaX with Co^{2+}. When using the initial concentration of 95.0% v/v ethanol, it was found that Co^{2+} modified zeolite NaA and zeolite NaX could increase the ethanol concentration to 99.1 - 99.8% v/v while the rest could increase only about 1%.

In the case of analcime and cancrinite, it was found that the percentage of ethanol was increased from 85.0% v/v up to 96.4 and 94.9% v/v, respectively. When the initial concentration of ethanol was 95.0% v/v, analcime and cancrinite could increase the ethanol concentration from 95.0% to 99.3 and 99.6% v/v, respectively.

School of Chemistry

Academic Year 2011

Student's Signature_____

Advisor's Signature_____

ACKNOWLEDGEMENTS

CONTENTS

CONTENTS (Continued)

CONTENTS (Continued)

LIST OF TABLES

LIST OF FIGURES

LIST OF FIGURES (Continued)

LIST OF ABBREVIATIONS

FT-IR	=	Fourier transform infrared spectrophotometer
XRD	=	X-ray diffractometer
ICP-MS	=	Inductively coupled plasma mass spectrometer
SEM	=	Scanning electron microscope
GC	=	Gas chromatography
FID	=	Flame ionization detector
°C	=	Degree Celsius
Å	=	Angstrom
% T	=	Percent transmittance
cm^{-1}	=	Per centimeter
g	=	Gram
mL	=	Milliliter
SUB	=	Secondary building units
SOD	=	Hydroxysodalite
FAU	=	Faujasite
DA	=	Diatomite treated with acid
DA-900	=	Diatomite treated with acid and calcined at 900 °C
DA-1100	=	Diatomite treated with acid and calcined at 1100 °C

CHAPTER I

INTRODUCTION

Today worldly price of crude oil rises nonstoply and has profound impact on economic world market. Thailand is not able to avoid this cycle. Consequently, it has led to find an alternative fuel to supplement petroleum use. Gasohol is one of the important alternative fuels, first initiated by His Majesty the King to reduce problems related to oil supply scarcity and falling of crop prices. Gasohol is a combination of ethanol with 99.5% purity ethanol and unleaded gasoline mixed at the volume ratio of 1:9. It is known that, even in fractional distillation of ethanol/water mixture, only 95% purity of ethanol was obtained due to an effect of azeotrope. To achieve 99.5% purity it is necessary to use some specific molecular sieves to remove 5% of water left. Based on this problem the aim of this research is to prepare molecular sieve that can be used to remove water from 95% ethanol. The expectation of the study is that zeolites synthesized from raw materials in Thailand and their modifications with metal ions will be served as highly efficient molecular sieves for eliminating 5% of water left in ethanol solution.

1.1 Zeolite

Zeolites are microporous crystalline aluminosilicates. The structure of zeolites contains aluminum, silicon, and oxygen in regular frameworks with cations and water in the pores. The silicon and aluminum are tetrahedrally coordinated with each other through shared oxygen atoms. Zeolite primary structures are tetrahedral of SiO_4 and

AlO_4 shown in Figure 1.1 Each AlO_4 tetrahedron in the framework bears a net negative charge which is balanced by a cation. The structure formula of zeolite is based on the crystallographic unit cell, the smallest unit of structure, represented as.

$$M_{x/n} \, [(AlO_2)_x \, (SiO_2)_y] \, . \, wH_2O$$
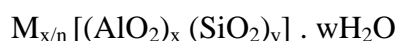
where M is an alkali or alkaline earth cation, n is the valence of the cation, w is the number of water molecules per unit cell, x and y are the total number of tetrahedra per unit cell, and the ratio y/x usually has values of 1 to 5. In the case of the high silica zeolite, y/x can be ranging from 10 to 100 (Guisnet and Gilson, 2001 and Barrer, 1998).

The composition of zeolite can be best described as having three components:

$$M^{m+}_{n/m} \, . \qquad [Si_{1-n}Al_nO_2]. \qquad nH_2O$$

extraframework cations   *freamework*   *sorbed phase*

The extraframework cations are ion exchangeable and give rise to the rich ion exchange chemistry of these materials. The novelty of zeolite stems from their microporosity and is a result of the topology of the framework (Ghobarkar, 2003; Payra and Dutta, 2003 and Xu, 2007). Because of such interesting properties, zeolite are widely used for molecular sieves.
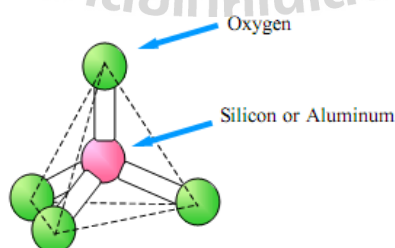
Figure 1.1 The primary building unit of zeolite structure.
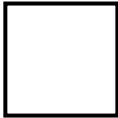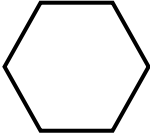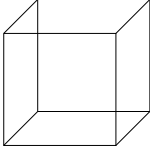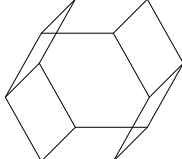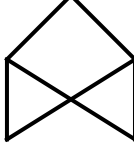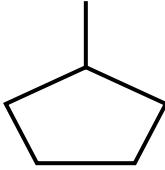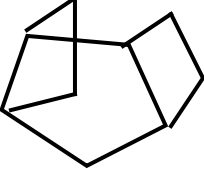
Zeolite framework structure types are commonly classified on the basis of constituent units (Meier, 1988). The primary building unit of a zeolite structure is the individual tetrahedral TO_4 units, where T is either Si or Al as shown in Figure 1.1. Primary tetrahedral unit of AlO_4 and SiO_4 are linked together by sharing oxygen as represented.

There are sixteen secondary building units, consisting of geometric groupings of those tetrahedra which can be used to describe all of the known zeolite structures. The framework of zeolite can be thought of as being made of finite component units or infinite component unite like chains and layers. The concept of infinite component units, such as secondary building units (SBU) are composed of 4, 5, 6, and 8-member single rings, 4-4, 6-6, and 8-8 member double rings, and 4-1, 4=1, 5-1, 5-2, 5-3, 6-1, 6-2, and 4-4=1 branch rings and spiro-5, as represented in Figure 1.2 (Szostak, 1998 and Xu, 2007). The SUBs, for various structure types of zeolites given in the database of zeolite structure are summarized in Table 1.1, shows a description of secondary building units and the shorthand notation for zeolite (King, 1994). One type of framework can comprise several SUBs. For example, in Figure 1.3 LTA framework (zeolite A) contains five types of SUBs, including 4, 8, 4-2, 4-4, and 6-2 units, any of which can be used to describe its framework structure.
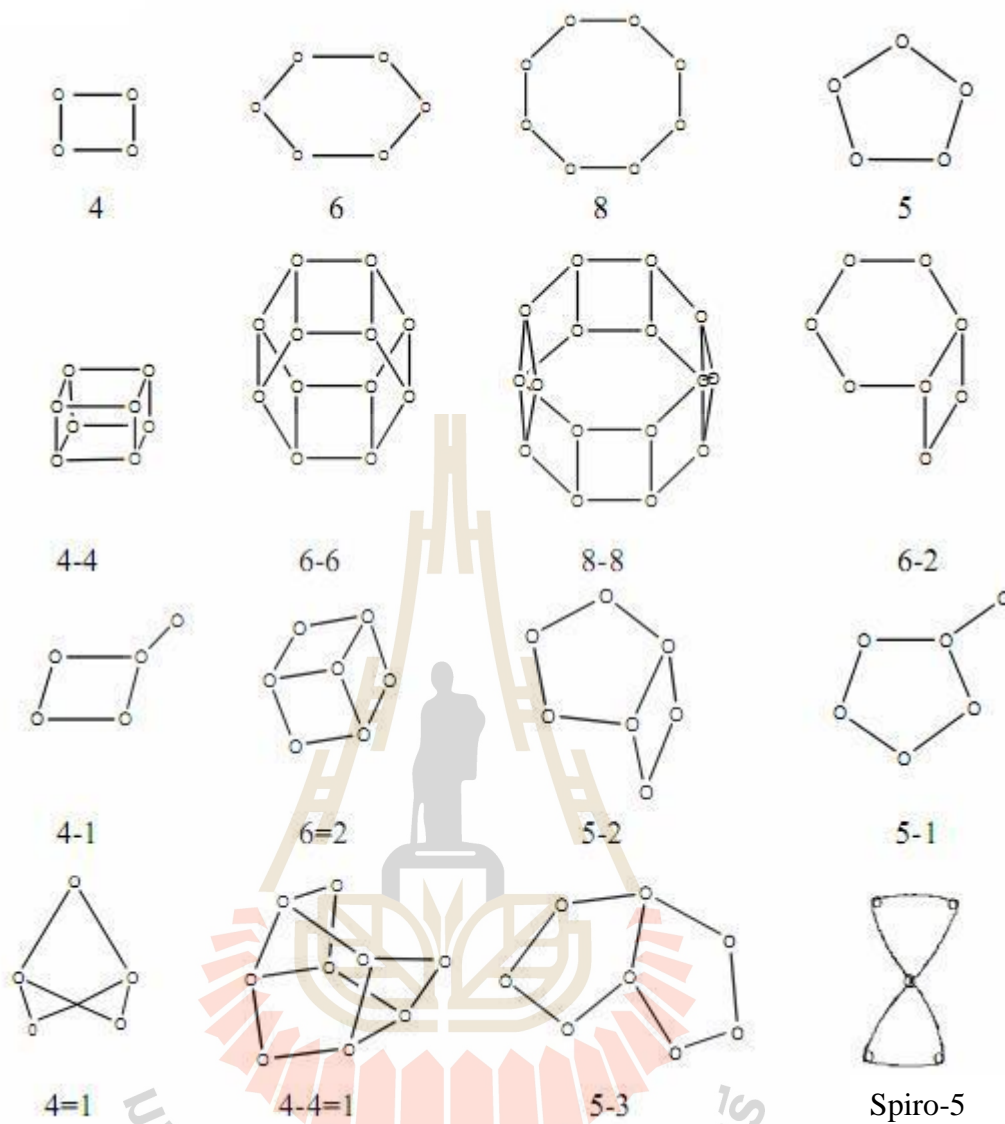
Figure 1.2 The secondary building units (SBU) in zeolite structures (Szostak, 1998).

Table 1.1 The seven groups of secondary building units (SBU) (Xu, 2007).

Group	Secondary building units (SBU)	Structure
1	Single 4-ring, S4R	
2	Single 6-ring, S6R	
3	Double 4-ring, D4R	
4	Double 6-ring, D6R	
5	Complex 4=1, T_5O_{10} unit	
6	Complex 5-1, T_8O_{16} unit	
7	Complex 4-1=1, $T_{10}O_{20}$ unit	

Primary units

Secondary building unit

Polyhedral building unit

Zeolite structures

Zeolite A   Sodalite   Zeolite X,Y
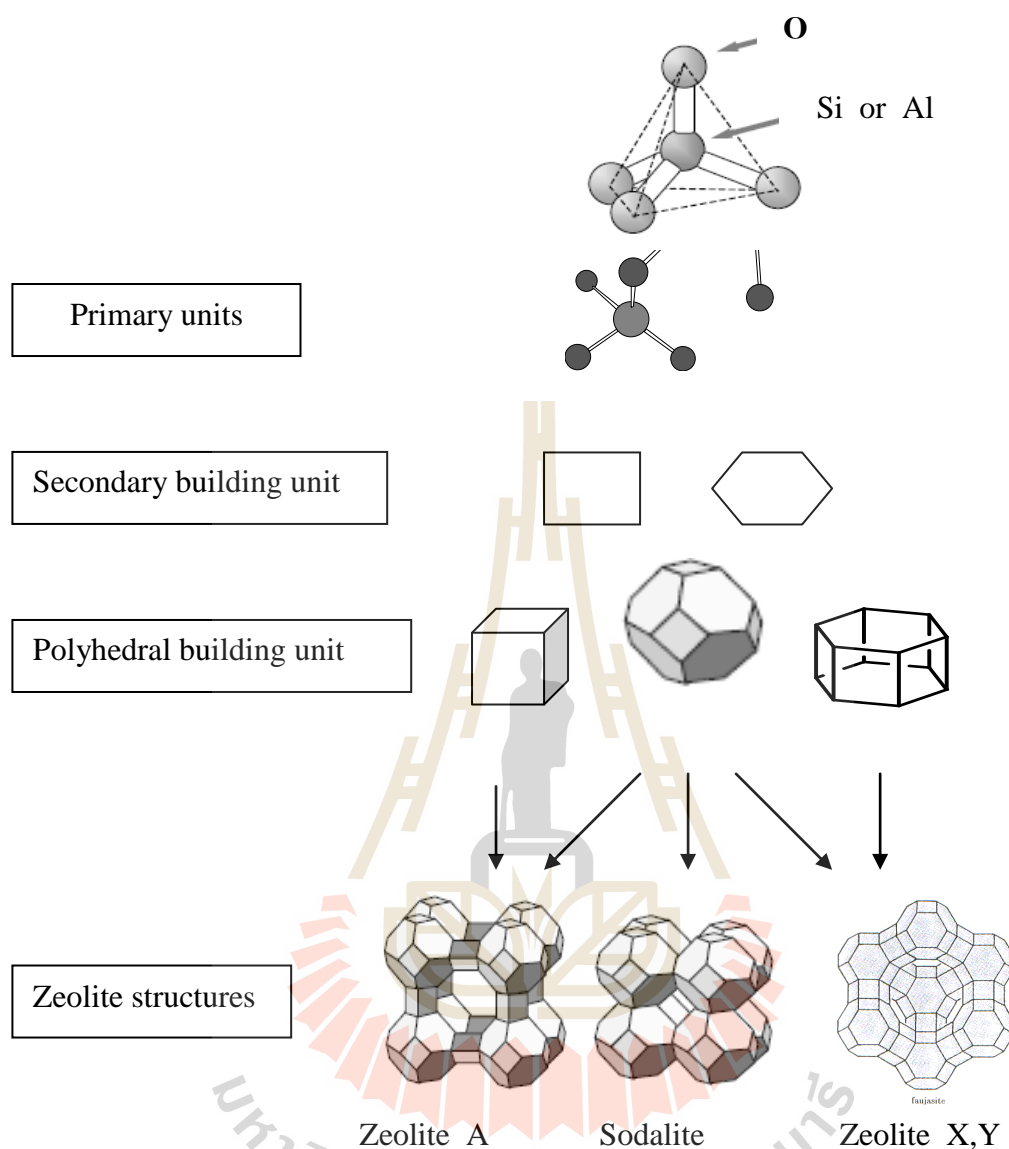
Figure 1.3   Formation of three common zeolites from   primary AlO_4 and SiO_4

tetrahedral units   through a combination of secondary ring unit and

different mixes of tertiary polyhedral.

1.2 Zeolite NaA

The Linde Type A (LTA) framework is related to SOD, but in this type, the

sodalite caged, in a primitive cubic arrangement, are joined via double 4-ring rather

than single ones. This creates an α - cage instead of a β – cage in the center of the unit

cell, and a 3-dimensional, 8-ring channel system. Alternatively, the framework can be described as a primitive cubic arrangement of α – cage joined through single 8-rings (producing a sodalite cage in the center). This is one of the more open zeolite framework types with a framework density of only 12.9 T-atoms per 1000 Å (Bekkum, 2001).

Zeolite NaA is the simplest synthetic zeolite with a molecular ratio of one silicon to one aluminuum to one sodium cation. Zeolite NaA exhibits the LTA (linde type A) structure. It has a cubic structure as shown in Figure 1.4. The pseudo unit cell of zeolite NaA consists of 12 SiO_2 and 12 AlO_2 units, with enclosing a large cavity (α cage) with diameter of 11.4 Å and small cavity (β cage) with diameter of 6.6 Å, and a pore window opening of 4.1 Å. The chemical composition of pseudo unit cell is $Na_{12}[Al_{12}SiO_{12}O_{48}] \cdot 27H_2O$. It is 1/8 of the true unit cell. Zeolite NaA is constructed from structures of hydroxysodalite (SOD) sharing with bridging oxygen ion between oxygen four atoms and SOD structure is constructed from sodalite cage. The relatively simple structure of sodium zeolite LTA and the related hydroxysodalite. Some properties of zeolite are very interesting such as high degree of hydration, low density and large void volume when dehydrated, stability of crystal structure, cation exchange properties, uniform molecular sized channels, special physical properties, i.e. high surface area and molecular sieve, adsorption for gas and vapor and catalytic properties. Due to its unique and special properties which are suitable for various kinds of chemical reactions, zeolite has been widely used in many applications. Zeolite NaA is of much interested for various applications such as detergency, desiccant, adsorption and separation, catalysis, and ion exchange.
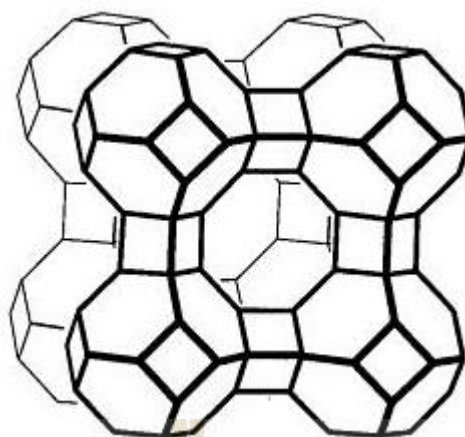
Figure 1.4 The LTA framework type (Bekkum, 2001).

1.3 Zeolite NaX

The Faujasite (FAU) framework type (Figure 1.3), in this type, they are arranged in the same way as the carbon atoms in daimond, and are joined to one another via double 6-ring. This creates the so-called supercage with four, tetrahedrally-oriented, 12-ring por openings, and a 3-dimensional channel system. The framework density, at 12.7 T-atoms per 1000 Å, is even lower than that of LTA. There is a center of inversion in each of the double 6-ring, so the puckered layers of sodalite cages are related to one another by inversion. The framework type can also be described as an ABCABC stacking of such layers (see Figure 1.5). The combination of large void volume (ca50%), 12-ring pore openings and 3-dimensional channel system makes the thermally stable silicate materials with the FAU framework type ideal for many catalytic applications (Bekkum, 2001).

Zeolite NaX is an aluminum-rich synthetic analogue of the naturally occurring mineral Faujasite (Figure 1.5) with the general formula $Na_2O \cdot Al_2O_3 \cdot nSiO_2 \cdot wH_2O$. When the value of n is 2-3; they are designated as zeolite X and those with higher values as zeolite Y. The large cavities (super cage, α cage, diameter = 13 Å) and sodalite cage cavities (β cage, diameter = 6.6 Å,with windows of 7.4 Å) are

interlocked to be a three dimensional network. The oxygen atoms lie approximately midway between each pair of Si and Al atoms, but are displaced from those points to give near-tetrahedral angles about Si and Al (S6R). The oxygen atoms are shared by sodalite units and super cages and may be viewed as entrances to the sodalite cavities. Each unit cell has eight sodalite units and eight super cages, 16 D6R, 16, 12-rings, and 32 S6R. Zeolite X has a wide range of industrial applications, partly because of its large pore size and void volume. Its sorptive and catalytic properties depend also on its exchangeable cations: its size, its charge, its chemical nature and its placement within the zeolite. Three main properties of zeolite are technologically important: they are selective and strong absorbents; they are selective ion exchanger and they are catalytically active. Other interesting properties associated with zeolites are their high thermal stability and their metal-oxygen tetrahedral that are exposed to the surface accessible for modification. Currently, they are useful for commercial applications such as being catalyst for hydrocarbon cracking, detergent builders, ion exchanger for removal of heavy metals, absorbent for separation and purification processes.
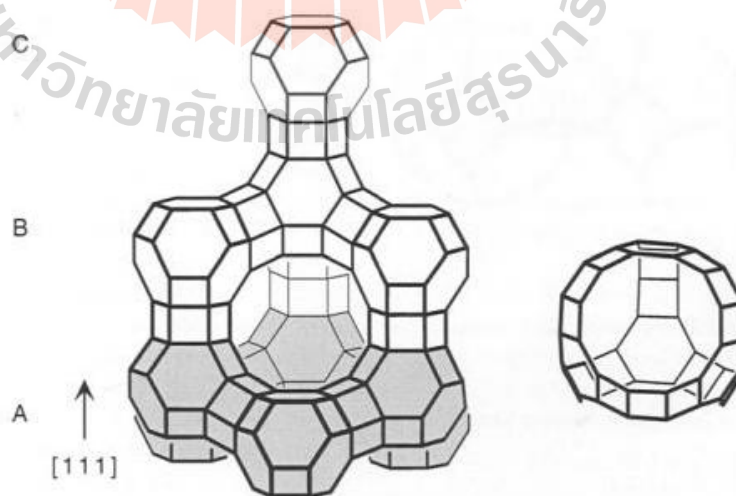
Figure 1.5 The FAU framework type and its supercage, the tree different layers of

sodalite cages are indicated with the letters A, B, and C (Bekkum, 2001).

1.4 Analcime

Analcime is found in deposits of various ages and types, in alter tuffs, sedimentary deposits, and in basic magmas. Whether analcime has preserved the isotopic composition from the time of formation depends on the age of the deposit, post-formation thermal history, and water/rock ratios (Faiia and Feng, 2000).

Analcime ($NaAlSi_2O_6.H_2O$) is the smallest-pore zeolite and occurs widely in hydrothermal and diagenetic environments (Gottardi and Galli, 1985). The crystal structure of analcime was one of the first zeolites to be determined. Analcime is consistent with secondary building units based on 4-ring, 6- rings and 6-2 rings. Its ideal crystal structure composes of 16 formula units in a cubic unit cell (space group Ia3d), with a random distribution of 16 Al and 32 Si atoms on the 48 tetrahedral positions and a random distribution of 16 Na atoms on the 24 channel positions. Framework O atoms are in 96 general positions, and the O atoms of the H_2O molecules are in 16 channel positions. Framework O atoms are shared between linked (Si, Al) tetrahedra to form an aluminosilicate framework composed of rings of six and four tetrahedra. Sodium is coordinated inside these channels by 4 framework oxygen atoms and two water molecules. Water is found in the centre of the largest pore cages. Upon dehydration, the sodium cations become less stable due to a lower coordination number and begin to move into the position that were initially occupied by the water molecules. It is possible that the sodium migration coupled with changing unit cell dimension blocks the external water vapor from reaching some of the framework oxygen sites. This prevents the bulk isotopic composition of analcime from reaching the expected equilibrium value. As the silica content increases, the sodium content decreases, and there is a concurrent linear increase in the number of H_2O molecules. This structure is similar to that of leucite ($KAlSi_2O_6$), which is tetragonal. The only difference is that the

larger K atoms in leucite occupy the H_2O 16 positions of analcime, instead of the Na 24 position reported diffusion coefficients for heulandite, chabazite, melinite and various sieve zeolites of the order of 100 thousand to 100 million times greater than that for analcime. Other zeolites can be expected to be greater in water content and internal surface area.

1.5 Cancrinite

Cancrinite belongs to the abc family of zeolites of which sodalite, chabazite, and offretite are also members. Cancrinite is a low-silica zeolite (Si/Al=1) that can be prepared synthetically from gels containing anions such as CO_3^{2-}, SO_4^{2-}. It can also be made in highly alkaline media containing only sodium or a combination of cations such as lithium and sodium or lithium and cesium. Cancrinite group (CAN) minerals are framework aluminosilicates and are characterized by an ordered distribution of Si and Al atoms in the tetrahedral sites. The framework consists of 6-ring windows, close-packed in an ABAB type of stacking sequence in the space group $P6_3$. Therefore, chains of undecahedral cages, also known as cancrinite cages, and 12-ring channels are formed along the 3-fold and 6_3-axes, respectively. The cancrinite cage is composed of two parallel 6-ring windows perpendicular to the c-axis, bounded by 6-ring and 4-ring windows. The 4-ring windows are shared by neighboring cages, while the 6-ring windows interlock to form the one-dimensional 12-ring channels. Extra-framework cations, such as Na^+, K^+, and Ca^{2+}, and water molecules are located both in the cancrinite cages and the 12-ring channels. Anionic species, such as OH^-, CO_3^{2-} and SO_4^{2-}, are usually occluded along the 12-ring channels. Due to the diverse compositional and structural combinations of anionic species and extra-framework cations, various structural models have been proposed for both mineral and synthetic

cancrinites. Aluminosilicate minerals, such as carbonate-cancrinite, basic cancrinite, davyne, vishnevite and microsommite, are illustrative of various salts or hydroxy-occluded cancrinites, while tiptopite is a natural beryllophosphate analogue of the basic cancrinite. Examples of synthetic cancrinites include sodium forms of carbonate-cancrinites, lithium-cesium and lithium-thallium forms of cancrinite-hydrates and other sodium forms of gallosilicate and aluminogermanate analogues. Both natural and synthetic cancrinites exhibit limited adsorption capacities due to blocking of the one-dimensional 12-ring channels, either by anionic species or by stacking faults. Removal of the occluded molecules often leads to the collapse of the 12-ring channels and the formation of sodalite or nepheline type structures.

1.6 Ethanol

Ethanol also called ethyl alcohol, pure alcohol, grain alcohol or drinking alcohol, is a volatile, flammable and colorless liquid. It is a psychoactive drug, best known as the type of alcohol found in alcoholic beverages. Absolute or anhydrous alcohol generally refers to purified ethanol, containing no more than one percent of water. It is needed for most industrial and fuel uses. By fractional distillation ethanol mixture can be concentrated to 95.6% by weight or 89.5% by mole. At this concentration it is not possible to remove remaining water from rectified spirit by straight distillation as ethyl alcohol forms a constant boiling mixture with water and is known as azeotrope. Therefore, special process for removal of water is required for manufacture of absolute alcohol. In order to extract water from alcohol it is necessary to use some dehydration, which is capable of separating water from alcohol.

The mixture of 95.6% ethanol and 4.4% water (percentage by weight) is an azeotrope with a boiling point of 78.2 °C, and cannot be further purified by distillation.

There are several methods used to further purify ethanol beyond 95.6%. Dehydration using unslacked lime (calcium oxide) is one example. Industrial alcohol is placed in a reactor and quick lime is added to that and the mixture is left over night for complete reaction. It is then distilled in fractionating column to get absolute alcohol. Water is retained by quick lime. This process is used for small-scale production of absolute alcohol by batch process. Dehydration using lime or a salt after distillation ethanol can be further purified by "drying" with lime or a hygroscopic material such as rock salt. When lime is mixed with the water in ethanol, calcium hydroxide is formed. The calcium hydroxide can then be separated from the ethanol. Similarly, a hygroscopic material will dissolve some of the water content of the ethanol as it passes through, leaving a purer alcohol (Mathewson, 1980).

Addition of an entrainer the ethanol-water azeotrope can be broken by the addition of a small quantity of benzene or cyclohexane. Benzene, ethanol and water form a ternary azeotrope with a boiling point of 64.9 °C. Since this azeotrope is more volatile than the ethanol-water azeotrope, it can be fractionally distilled out of the ethanol-water mixture, extracting essentially all of the water in the process. The bottoms from such a distillation is anhydrous ethanol, with several parts per million residual benzene. Benzene is toxic to human and cyclohexane has largely supplanted benzene in its role as the entrainer in this process. However, this purification method leaves chemical residues which render the alcohol unfit for human consumption (Mathewson, 1980).

Membranes can also be used to separate ethanol and water. The membrane can break the water-ethanol azeotrope because separation is not based on vapor-liquid equilibrium. Membranes are often used in the so-called hybrid membrane distillation process. This process uses a pre-concentration distillation column as first separating step. The further separation is then accomplished with a membrane operated either in

vapor permeation or pervaporation mode. Vapor permeation uses a vapor membrane feed and pervaporation uses a liquid membrane feed.

Pressure reduction at pressures less than atmospheric pressure, the composition of the ethanol-water azeotrope shifts to more ethanol-rich mixtures, and at pressures less than 70 torr, there is no azeotrope, and it is possible to distill absolute ethanol from an ethanol-water mixture. While vacuum distillation of ethanol is not presently economical, pressure-swing distillation is a topic of current research. In this technique, a reduced-pressure distillation first yields an ethanol-water mixture of more than 95.6% ethanol. Then, fractional distillation of this mixture at atmospheric pressure distills off the 95.6% azeotrope, leaving anhydrous ethanol at the bottoms.

Alternatively a molecular sieve can be used to selectively adsorb the water from the 95.6% ethanol solution. Synthetic zeolite in pellet form can be used, as well as a variety of plant-derived adsorbents, including cornmeal, straw, and sawdust. The zeolite bed can be regenerated essentially an unlimited number of times by drying it with a blast of hot carbon dioxide. Cornmeal and other plant-derived adsorbents cannot readily be regenerated, but where ethanol is made from grain, they are often available at low cost. Dehydration with molecular sieve process, the rectified spirit from the rectifier is superheated with steam in feed super-heater. Super-heated rectified spirit from feed super-heater is passed to one of the pair of molecular sieve beds for several minutes. On a timed basis, the flow of superheated rectified spirit vapor is switched to the alternate bed of the pair. A portion of the anhydrous ethanol vapor leaving the fresh adsorption bed is used to regenerate the loaded bed. A moderate vacuum is applied by vacuum pump operating after condensation of the regenerated ethanol water mixture. This condensate is transferred from recycle drum to the rectified column in the hydrous distillation plant via recycle pump. The net make of anhydrous absolute alcohol draw is condensed in product condenser and passed to product storage. The life of molecular

sieve may be around five to seven years. However, the operating cost is considerably less than azeotrope distillation. Most of the ethanol dehydration plants for production of absolute alcohol are based on azeotrope distillation. It is a mature and reliable technology capable of producing a very dry product (Lei, Wang, Zhou, and Duan, 2002)

1.7 Research objectives

1. To synthesize analcime and cancrinite from raw diatomite and modified diatomite which were treated with acid and heat.

2. To synthesize zeolite NaA and zeolite NaX from kaolin and to modify zeolite NaA and zeolite NaX with cations.

3. To characterize the starting materials and the synthesized sodium zeolites samples in by different techniques.

4. To investigate the water removal in ethanol solution (85% and 95% v/v) by the synthesized sodium zeolites and cationic modified zeolite NaA and zeolite NaX.

CHAPTER II

LITERATURE REVIEWS

2.1 Synthesis of sodium zeolites

In the present the synthesis of zeolites from low-cost silica-alumina sources has been interested from many researchers. The natural materials such as volcanic, glasses, volcanic vitric ashes, rocks, fly ash, rice husk and clay minerals have been frequently used as silica-alumina sources for zeolite formation due to their high contents of silica and aluminum, which are easily dissolved and recombined to transform into zeolites under the alkali hydrothermal conditions.

Rocha and Adams (1991) studied the synthesis of zeolite NaA from metakaolinite treated with a strong base of 5 M NaOH. The aluminous matrix of metakaolinite transforms very rapidly, even at room temperature, and five- and six-coordinated Al are converted into four-coordination. The siliceous matrix of kaolinite is partially preserved in metakaolinite and is responsible for the residual long-range order in the ab plane. The aluminous matrix of metakaolinite prepared by calcined kaolinite at 700 °C is more strongly affected by the alkali when the populations of four- and five- coordinated Al are at a maximum and the population of six-coordinated Al at a minimum. Upon treatment with alkali, metakaolinite slowly dissolves. SiO_4^{4-} and $Al(OH)_4^-$ ions in solution condense to an amorphous phase with Si/Al = 1. This direct precursor transforms into zeolite A by a solid-state rearrangement.

Gualtieri, Norby, Artioli, and Hanson (1997) used time resolved synchrotron powder diffraction techniques to study the kinetics of zeolite A from natural kaolinite activated at 800 °C with 4 M NaOH at reaction temperature of 70 - 100 °C. They found that the formation of zeolite A was depended on the calcinations of starting material but not depended on the number of defects of the starting material. The results of the kinetic analysis are interpreted in the light of the structural state of the starting kaolinite, and of the temperature of activation of the precursor material. For kaolinite activated at high temperature the nucleation and crystallization of zeolite A is essentially independent of the defect density of the original kaolinite, and the thermal history of the precursor seems to be the main controlling parameter. The formation process of zeolite A from metakaolinite materials obtained at lower activation temperatures shows significantly faster reaction rates and lower apparent activation energies. This is again interpreted in the light of the short range inhomogeneities present in metakaolinite. As the reaction proceeds metastable zeolite A transforms intohydroxy-sodalite.

Qiu and Zheng (2009) studied the removal of lead, copper, nickel, cobalt, and zinc from water by a cancrinite-type zeolite synthesized from fly ash. In this study, a cancrinite-type zeolite (ZFA) was synthesized from Class C fly ash via the molten-salt method. The adsorption equilibriums of Pb^{2+}, Cu^{2+}, $Ni^{2}+$, Co^{2+}, and Zn^{2+} on ZFA were studied in aqueous solutions and well represented by Langmuir isotherms. The increase of pH levels during the adsorption process was suggested that the uptake of heavy metals on ZFA was subjected to an ion exchange mechanism. It was found that the maximum exchange level (MEL) follows the order: Pb^{2+} (2.530 mmol/g) > Cu^{2+} (2.081 mmol/g) > Zn^{2+} (1.532 mmol/g) > Co^{2+} (1.242 mmol/g) > Zn^{2+} (1.154 mmol/g). Comparison with previous studies, the MEL of ZFA is higher than that of the commonly used natural zeolites and it is also comparable to (or higher than) several

synthetic zeolites and ion exchange resins. The high MEL of heavy metals on ZFA is attributed to the high cation exchange capacity (CEC) and proper pore size of cancrinite. The pseudo-first-order kinetics suggests that the ion exchange processes were diffusion-controlled.

Atta, Jibril, Aderemi, and Adefila (2012) synthesized analcime zeolite by a hydrothermal technique with rice husk ash and metakaolin as silica and alumina sources. It was found that analcime was obtained after 72 hours of aging and 24 hours of reaction time at 180°C.

2.2 Modification of zeolites

There are many studies on the modification of zeolites and clay minerals with cations. The ion exchange behavior of various inorganic exchangers and other types of crystalline silicates such as clay minerals and feldspathoids has been extensively reviewed. Because of their three-dimensional framework structure, most of zeolites and feldspathoids do not undergo any appreciable dimensional change with ion exchange. Clay minerals, because of their two-dimensional structure, may undergo swelling or shrinking with cation exchange. One application for commonly occurring zeolite mineral minerals (such as clinoptilolite) is in the selective removal of radioactive ions from radioactive waste materials.

The cation exchange behavior of zeolites depends upon the nature of the cationic species, the cationic size in both anhydrous and hydrated form, temperature, concentration of the cation species in solution, solvent (most exchange has been carried out in aqueous solution, although some work has been done in organic solvents) and the structural characteristics of the particular zeolite. Cation selectivity in zeolites do not follow the typical rules that are evidenced by other inorganic and

organic exchangers. Zeolite structures have unique features that lead to unusual types of cation selectivity and sieving. The recent structural analysis of zeolites forms a basis for interpreting the variable cation exchange behavior of zeolites.

The ion exchange processes of zeolite are defined by:

$$Z_A B^{z_B^+}_{(z)} \; + \; Z_B A^{z_A^+}_{(s)} \quad \Leftrightarrow \quad Z_A B^{z_B^+}_{(s)} \; + \; Z_B A^{z_A^+}_{(z)}$$
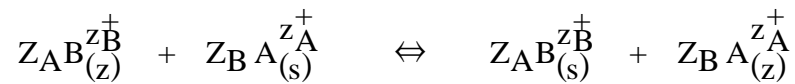
Where Z_A, Z_B are the changes of cations A and B and the subscripts z and s refer to the zeolite and solution, respectively. The position of the equilibrium is a measure of the ion-exchange selectivity. The selectivity for given cations is determined by the electric fields of the coordinating anionic locations in the zeolite framework. Thus, for each zeolite type there is a specific selectivity series with the cations arranged in order of increasing exchange ability.

Maes and Cremers (1974) studied the ion exchange of the divalent transition metal ions of Co, Ni, Cu and Zn on synthetic NaX and NaY zeolites. They studied at 0.01 N at 5, 25, and 45 °C. In spite of the near identical crystal radius of the 4 ions, there is a marked difference in the exchange isotherms. The maximum loading limits are temperature dependent and not consistent with the static model of a definite exchange capacity in the big cavities, i.e., 82% and 68% in X and Y respectively. The selectivity in the small cages depends on the occupancy and type of ion present in the big cavities and vice versa. The overall selectivity of both X and Y zeolite for bivalent transition metal ions increases in the order Ni < Co < Zn < Cu. In addition to the ion hydration characteristics and ionic radius the exchange is governed by the coordination ability of the transition metal ion.

Richard and Rodney (1975) studied the ion exchange of Mn^{2+}, Co^{2+}, Ni^{2+}, Cu^{2+}, and Zn^{2+} in ammonium mordenite over a pH range of 4 - 7 at 25 °C. The values of the thermodynamic equilibrium constant K_a and the standard free energy of exchange

$\Delta G°$ were calculated for reversible systems. There were no any cases that at 25 °C the degree of exchange of metal ions exceed 50% and pH and anion were found to have no significant effect on the equilibria. A thermodynamic affinity sequence of $Mn^{2+} > Cu^{2+} > Co^{2+} \sim Zn^{2+} > Ni^{2+}$ was established and thermodynamic affinities of the zeolite for pairs of metal ions were calculated using the triangle rule. Selectivity quotients indicated that mordenite would preferentially remove manganese (II) or copper (I1) from a binary solution mixture of one of these ions with cobalt (II), nickel (II) or zinc (II).

Minati and Dibyendu (1982) studied the ion exchange behaviour of some divalent transition metal ions M^{2+} (Zn^{2+}, Cu^{2+}, Ni^{2+}, Co^{2+}, Mn^{2+}) in a zeolite NaX at intermediate stages before equilibrium. The equivalent counter ion supplied in the solution, given by the equivalent ratio of the two counter ions $2M^{2+}/Na^+$, was found to be critical in determining the saturation level of exchange. The series of relative abilities of exchange was very similar to the well known selectivity series at equilibrium. It was suggested that water exchange of the metal ions in solution could be one of the factors controlling the relative ease of ion exchange.

2.3 Ethanol dehydration

It is known that even in fractional distillation of ethanol - water mixture, it yields only 95.6% pure ethanol due to an effect of azeotrope. To purify ethanol from the mixtures in most research works has been done under various technologies such as azeotrope distillation (Wang et al., 2002), pressure swing absorption (Yang, 1987; Carmo and Gubulin, 2002 and Pruksathorn and Vitidsant, 2009), pervaporation process (Aouinti and Belbachir, 2008 and Sato et al., 2008), liquid phase absorption

(Xien Hu, 2001; and Beery and Ladisch, 2001) and molecular sieve (Sowerby and Crittenden, 1988; Teo and Ruthven, 1986 and Hassaballah and Hills, 1990).

Sowerby and Crittenden (1988) studied the recovery of dry ethanol in the vapour phase of the composition around that of the azeotrope by using fixed beds packed with 3A, 4A, 5A, and 10A molecular sieves. For the similar adsorption and desorption conditions, the water capacity of 4A molecular sieve was found to be greater than that of 3A molecular sieve. A longer length and a larger amount of heat released during adsorption confirmed that 3A molecular sieve presents a greater resistance to the uptake of water than 4A molecular sieve. Consequently, the amount of desorbed water under similar conditions, was found to be greater for 4A than that for 3A molecular sieve. The experimental results of water desorption indicated that the rate of removal of water from 4A is slightly greater than that from 3A molecular sieve. This again infers that 3A molecular sieve presents a greater resistance to the movement of water than 4A molecular sieve. For equivalent duties, an adsorption column packed with 4A molecular sieve would be smaller and would also require a reduced energy input when compared to one packed with 3A molecular sieve.

Teo and Ruthven (1986) studied the dehydration adsorption of aqueous ethanol using 3A molecular sieves adsorbent. The experiment was done by following the uptake curves for a closed batch system and by measuring breakthrough curves for a packed column. This system is potentially attractive for the dehydration of rectified spirit by adsorbing the water on 3A molecular sieves. It was found that the uptake rate was controlled primarily by intraparticle pore diffusion resistance with some additional contribution from external film resistance, depending on the hydrodynamic conditions. The equilibrium isotherm is almost rectangular, and the kinetic data for both systems can be satisfactorily correlated in terms of simple kinetic models. The breakthrough curves for this system are well predicted by the model of Weber and

Chakravorti which therefore provides useful guidance for the design and economic evaluation of a larger scale unit.

Ladisch et al. (1984) studied the dehydration adsorption of ethanol–water mixture in the vapour phase using cornmeal absorbent. Ethanol vapors of 49.1%-98.4% were passed over cornmeal in the bench-scale column. A product of 99.6% by weight of ethanol was initially obtained. The cornmeal absorbent for dehydration of other alcohols was obtained when vapors of 71.5% n-propyl alcohol at 97.4 °C , 86.2% isopropyl alcohol at 85.8 °C and 88.9% tert-butyl alcohol at 87.6 °C. The preliminary data indicated that corn or other polysaccharide materials may have been found a use for dehydrating other industrially important alcohols. Applications involving other water/organic mixtures could also be postulated. Corn is a potentially attractive adsorbent for removing water from alcohols.

Hassabaiiah and Hills (1990) studied the dehydration adsorption of ethanol - water mixture using cornmeal absorbent. Experiments have been carried out on a laboratory-scale. The effects of varying particle size, feed concentrations and flow rates were investigated as well as regeneration conditions on the product quality and breakthrough times. It was found that 85% (w/w) vapor feed gave the best product and the product yields of up to 99.8% (w/w) alcohol were obtained at 0.85 mm particles. The energy costs as low as 4.0 MJ kg^{-1}. It is suggested how this figure could be improved at 90 °C. The corn meal studied was almost certainly gelatinized to a large extent, which reduced its selectivity. The further studies are undertaken to find the most selective adsorbent, which will then be tested to find its optimum regeneration parameters. A very considerable energy saving is envisaged over conventional distillation.

Al-Asheh, Banat and Al-Lagtah (2004) studied the separation of the ethanol - water azeotrope using of new biobased adsorbents and molecular sieve. Molecular

sieves of type 3A, type 4A and type 5A and biobased adsorbents such as natural corncobs, natural and activated palm stone and oke were used in the study. Each of these adsorbents was packed in a column, which was surrounded by a heating jacket. The water concentration in the feed solution was varied from 5% to 12% (weight basis). Experimental results of water sorption on molecular sieves and biobased adsorbents showed that adsorptive distillation could be used for separation of an ethanol–water system. The breakthrough results of water sorption on molecular sieves showed that type 3A molecular sieves gave good results in terms of breakthrough time and average outlet water concentration compared to those of type 4A and type 5A molecular sieves. Among the biobased adsorbents developed in this work, natural palm stone showed good results compared to those of other biobased adsorbents. Other biobased adsorbents gave better results in terms of breakthrough time and average outlet water concentration when compared to that of type 5A molecular sieves, except for activated oak.

Yamamoto et al. (2012) examined the adsorption characteristics of zeolites with different framework structures and different exchanged cation species with a view to using zeolites as adsorbents for the dehydration of ethanol. They measured the adsorption isotherm of water vapor on zeolites, the differential heat of the water-vapor adsorption, the liquid-phase adsorption isotherm of water in ethanol and packed bed breakthrough curves (BTC) for the adsorption of water in ethanol. As a result, they confirmed that an LTA or FAU zeolite exchanged with a monovalent cation species, such as a sodium cation or a potassium cation, showed a strong affinity to water in ethanol. The result of fitting the calculated BTC to the experimental result, they could estimate the intra-particle diffusion coefficient of water in a zeolite particle in terms of the adsorptive dehydration of ethanol. FAU-Na showed the largest adsorption capacity for water in ethanol.

In this research, the different types of zeolite molecular sieves were synthesized and utilized for removal of water from ethanol solution in order to increase the ethanol concentration at least up to 99.5%.

CHAPTER III

MATERIALS, INSTRUMENTATIONS AND

EXPERIMENTAL METHODS

This chapter is divided into three parts. In the first part, it refers to materials lists, instrumentations and experimental methods. The material lists are presented as chemicals, material, glassware and apparatus. The second part of the chapter describes about the experimental methods and the third part is the analytical instruments to characterize the samples, such as x-ray fluorescence (XRF), powder x-ray diffractometer (XRD), fourier transform infrared spectrometer (FTIR), scanning electron microscope (SEM), gas chromatograph (GC) and inductively coupled plasma spectrometer (ICP).

3.1 Material Lists

3.1.1 Chemicals and Materials

- Diatomite sample of Ban Keuw Mae Tha District, Lampang Province, Thailand (Sriphum Wattana Ltd.)

- Kaolin, Sibelco minerals (Thailand) Co, Ltd

- Anhydrous sodium hydroxide pellets, NaOH, Merck, Germany

- Aluminium hydroxide, $Al(OH)_3$, Aldrich, USA

- Sulfuric acid, H_2SO_4, Merck, Germany

- Ethanol absolute, C_3H_3OH, Merck, Germany

- Potassium chloride, KCl, Analytical reagent APS Ajax, Finechem, Australia

- Magnesium chloride, $MgCl_2 \cdot 6H_2O$, Analytical reagent APS Ajax, Finechem, Australia

- Calcium chloride, $CaCl_2 \cdot 2H_2O$, Laboratory reagent APS Ajax, Finechem, Australia

- Strontium chloride, $SrCl_2 \cdot 6H_2O$, Analytical reagent APS Ajax, Finechem, Australia

- Cupper (II) chloride, $CuCl_2 \cdot 2H_2O$, Analytical reagent APS Ajax, Finechem, Australia

- Cobal (II) chloride, $CoCl_2 \cdot 6H_2O$, Analytical reagent APS Ajax, Finechem, Australia

- Nickel chloride, $NiCl_2 \cdot 6H_2O$, Laboratory reagent APS Ajax, Finechem, Australia

- Zinc chloride, $ZnCl_2$, Laboratory reagent APS Ajax, Finechem, Australia

3.1.2 Glasswares

- Breakers 50, 100, 250, 500, 1000 mL

- Erlenmeyer flasks 125, 250 mL

- Volumetric flasks 25, 50, 100, 250, 500, 1000 mL

- Volumetric pipets 1, 5, 10, 25, 50 mL

- Round bottom flask 250 mL

- Condenser for reflux procedure

- Conical flask 125 mL

- Watch glass

- Utility clamp

- Glass stirring rod

- Mortal and pestle

3.1.3 Apparatus

- Heating mantle with stirrer (Horst)

- Vacuum filtration apparatus

- Oven for drying sample (Memmert)

- Furnace chamber (Carbolite CWF 12/23)

- Electronic dry cabinet (Dry-100, Weifo, Taiwan)

- pH meter, (Mettler Delta 320)

- Shaking water bath, (Maxi-Shake, Heto Lab Equipment, Denmark)

- Glass microfiber filters, Whatman GF/C diameter 47 mm

- Analytical balance, (Model 250A, Precisa, Switzerland)

- Digestion bomb

- Thermometer

3.2 Instruments

- Gas chromatography (GC), (Model HP6890)

- Powder X-Ray diffractometer (XRD), (Model D5005, Bruker)

- Fourier transform infrared spectrophotometer (FT-IR), (Model spectrum GX, Perkin-Elmer)

- X-Ray fluorescence spectrometer (XRF), (Model ED2000, OXFORD)

- Scanning electron microscope (SEM), (Model JSM-6400, JEOL)

- Inductively coupled plasma spectrometer (ICP), (Model Alilent 7500, Octapole Reaction System)

3.3 Experimental methods

3.3.1 Diatomite and kaolin preparations

Diatomite and kaolin samples were ground and sieved through the metal sieve with 230 mesh. The fraction less than 63 μm in size was used as starting material for further experimental. Diatomite and kaolin samples were characterized by WDXRF to find the compositions.

3.3.2 Acid and calcinations treatment

The condition of the treatment was performed according to the report of Apilak. 10 g of diatomite was mixed with 50 mL of 6 M H_2SO_4 and refluxed at 100 °C for 48 hours to eliminate ferric oxide. Then the solid was washed with deionized water until pH 7 and dried at 110 °C and it was denoted as DA (diatomite treated with acid). Afterward, DA samples were heated at 900 °C and 1100 °C for 5 hours and denoted as DA-900 and DA-1100, respectively.

3.3.3 Synthesis of analcime and cancrinite

The synthesis was carried out according to the report of Chaisena. DA, DA-900 and DA-1100 were used as silica sources. In the synthesis, 0.235 g of $Al(OH)_3$ was added into the mixture of 10% w/v of NaOH and silica sources with the ratio of solid to liquid 1:10 (in g : mL). The reaction mixture was carried out in digestion bombs at autogenous pressures at 140 °C with the reaction time of 120 hours. In the synthesis of cancrinite, the following condition was employed: 20% w/v

of NaOH with the ratio of solid to liquid 1:30 (in g : mL) and 0.2350 g Al(OH)$_3$ was added reaction temperature of 180 °C and reaction time 72 hours. The solid product was filtered and washed with deionized water to remove excess alkali until the pH 7, then it was dried at 110 °C.

3.3.4 Synthesis of zeolite NaA

Kaolin was used as alumina and silica source to synthesize zeolite NaA and the synthesis condition was based on Wongwiwattana. Briefly on the synthesis, kaolin was calcined at 700 °C for 1 hour and was reacted with 10% w/v of NaOH solution with the ratio of 1 g : 5 mL and the mixture was crystallized by reflux at 70 °C for 24 hours, afterwards the solid product was washed with deionized water until the filtrate was pH 7 and dried at 110 °C.

3.3.5 Synthesis of zeolite NaX

The synthesis of zeolite NaX from kaolin was done according to Thammavong. Kaolin was calcined at 900 °C for 1.5 hours. Then it was reacted with Na$_2$SiO$_3$ 1.5 g and 20 mL of 7.5% w/v NaOH solution and shaken at room temperature for 72 hours, then the mixture was crystallized at 90 °C for 24 hours. The solid product was washed with deionized water until the filtrate was pH 7 and dried at 110 °C.

3.3.6 Cationic modification of zeolite NaA and zeolite NaX

Synthesized zeolite NaA and zeolite NaX were modified with K$^+$, Mg^{2+}, Ca^{2+}, Sr^{2+}, Cu^{2+}, Co^{2+}, Ni^{2+}, and Zn^{2+} cations by ion exchange process. In the preparation 1.0 g of zeolites was mixed with 100 mL of 0.20 M chloride solutions of K$^+$, Mg^{2+}, Ca^{2+}, Sr^{2+}, Cu^{2+}, Co^{2+}, Ni^{2+}, and Zn^{2+} and shaken at room temperature for

24 hours. The solid product was washed with deionized water to free chloride and dried at 110 °C.

3.3.7 Characterization of treated samples and zeolites

The treated samples and the products were characterized by FT-IR spectroscopy (Perkin-Elmer Spectrum GX). FT-IR Spectrum was recorded in the region of 4000 - 400 cm^{-1} with the KBr pellet technique. X-ray diffractograms were recorded by Bruker D5005, operating at 40 kV with 40 mA with Cu-Kα radiation source and SEM micrographs were obtained with JEOL JSM-6400 scanning electron microscope. ICP-MS (Agilent 7500 ICP-MS) was used for the determination of cationic contents in zeolites samples. The instrument was calibrated using multi-element standards solutions prepared in 5% nitric acid (Merck) by mixing and diluting stock solutions of individual elements (Merck).

3.3.8 Adsorption of water in ethanol solution by zeolites

In the adsorption study the initial concentrations of 85 and 95% (v/v) ethanol solution were used. 1.0 g of zeolite was mixed with 100 mL ethanol solution and shaken at 30 °C for 24 hours. Then the solution was used to examine the concentration of ethanol. The solution was analyzed by gas chromatography with the condition as follows:

Column	Capillary Column HP-INNOWax Polyethylene Glycol
Detector	FID
Temperature	250 °C
Hydrogen flow	40.0 mL/min
Air flow	300.0 mL/min

Oven	Post temp 40 °C
Run time	3 mim
Volume of sample injection	0.4 µL

3.4 Characterization techniques

3.4.1 X-ray fluorescence

XRF is an elemental analysis technique with unique capabilities including highly accurate determinations for major elements and a broad elemental survey of the sample composition without standards. High energy photons (x-rays) displace inner shell electrons. Outer shell electrons then fall into the vacancy left by the displaced electron and normally emit light (fluoresce) equivalent to the energy difference between the two states. Since each element has electrons with more or less unique energy levels, the wavelength of light emitted is characteristic of the element. The intensity of light emitted is proportional to the elements concentration.

3.4.2 Powder X-ray Diffraction

Power diffraction is mainly used for the identification of compounds by their diffraction patterns. X-ray are used to study the internal structure of objects that are opaque to visible light but transparent to x-rays. The wavelength, most commonly used in crystallography, range between ~0.5 and ~2.5 Å since they are of the same order of magnitude as the shortest interatomic distances observed in both organic and inorganic materials. An X-ray diffraction has been used in two main areas; the fingerprint characterization of crystalline materials for identification and the determination of their structures, i.e. how the atoms packed together in the crystalline state and what the inter-atomic distance and angle are. These unique properties make

X-ray diffraction one of the most important characterization tools used in solid state chemistry and material science. An important equation for X-ray diffraction is Bragg's equation, which is derived geometrically in Figure 3.1. Bragg's equation shows a relationship between X-ray wavelength (λ) with lattice point distance (d) and the incident diffraction angle (θ).

$$n\lambda = 2d_{hkl}\sin\theta_{hkl}$$

The different crystal plane (hkl) in the crystal will diffract X-ray at different angle according to the Bragg's equation. Therefore, by rotating the sample plane with respect to the incident X-ray, the diffracted angles can be recorded by a detector and the diffraction pattern is obtained. The identification of the sample structure can be done by comparing the spectrum with the pattern stored in the database (Pecharsky and Zavalij, 2003).
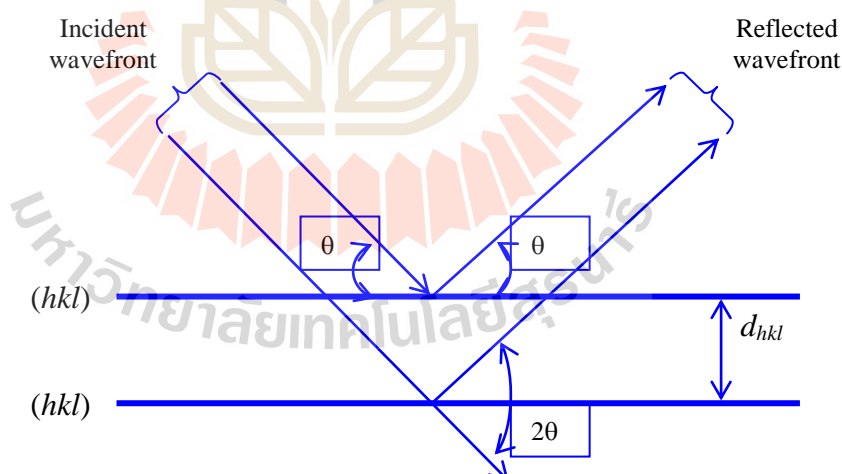
Figure 3.1 Geometrical illustration of the Bragg's equation.

3.4.3 Fourier transform infrared spectroscopy

Infrared spectroscopy is the study of the interaction infrared light with matter. Light is composed of electric and magnetic waves. The radiation in the vibration infrared region of the electromagnetic spectrum in terms of a unit called a

wavenumber (W), rather than wavelength (λ). Wavenumbers are expressed as reciprocal centimeters (cm-1). The wavenumber of a light is defined as the reciprocal of the wavelength.

$$W = 1/\lambda$$

Fourier transform infrared (FTIR) spectroscopy measures dominantly vibrations of functional groups and highly polar bonds. Thus these chemical fingerprints are made up of the vibrational features of all the samples components.

The majority of FTIRs operate in mid infrared radiation will be defined as light between 4000 and 400 cm^{-1}. FTIR experiments generally can be classified into thefollowing two categories: (a) qualitative analysis, where the aim is to identify the sample and (b) quantitative analysis, where the intensity of absorptions are related to the concentration of the component. Potassium bromide (KBr) pellets are used to obtain the infrared spectra of solid, and are particularly to powdered sample. KBr is an inert, infrared transparent material and acts as a support and a diluent for the sample.

3.4.4 Scanning Electron Microscopy

Scanning electron microscope (SEM) is a type of microscope that uses electrons rather than light to form an image. The SEM does not produce a true image of the specimen. Instead, SEM produces a point by point reconstruction of the specimen, basically the same way a television set reconstructs an image from signals sent by the television station transmitter. SEM reconstructs image of the specimen from a signal emitted from the specimen when it is illuminated by the high-energy electron beam, instead of a signal from the television transmitter. The preparation of samples is relatively easy since most SEM instruments only require the sample to be conductive. The combination of higher magnification, larger depth of focus, greater

resolution and ease of sample observation make SEM one of the most heavily used instruments in present-day research. The samples must be a conductive material in order to be able to interact with an electron; SEM samples are coated with a very thin layer of gold by a machine called a sputter coater. The SEM shows very detailed 3-dimentional images at a much higher magnification than is possible with a light microscope.

The image in the scanning electron microscope is produced in basically the same way, except that, instead of the signal coming from the television station transmitter, the signal now comes from the interaction of an electron beam with the specimen in the column of the SEM.

A detector counts these electrons and sends the signals to an amplifier. The final image is built up from the number of electrons emitted from each spot on the sample. By this way, the morphology of the sample can be seen directly from the micrograph (Lee, 1993).

3.4.5 Gas chromatography

Gas chromatography is a technique used to separate, identifiy and quantify volatile organic compounds in a sample matrix.

Principle

Gas chromatography is based on the repeated partition or adsorption, between a mobile phase and a stationary phase, of components to be separated. The mobile phase is always a gas, known as the carrier gas. The stationary phase can be either a solid or a liquid. A very small amount of liquid mixture is injected into the intrument and is volatilized in a hot injection chember. The volatile organic compounds are carrier through the stationary phase by the flow of the carrier gas. The saparation based on differences in migration rates among the sample components. The volatile

organic compounds are separated by differences in their partitioning behavior between the mobile gas phase and the stationary phase in the column into pure components.

Intrument

In summary, a gas chromatograph functions as follows. An inert carrier gas flows continuously from large gas cylinder through the injection port, the column, the detector and data recorder.
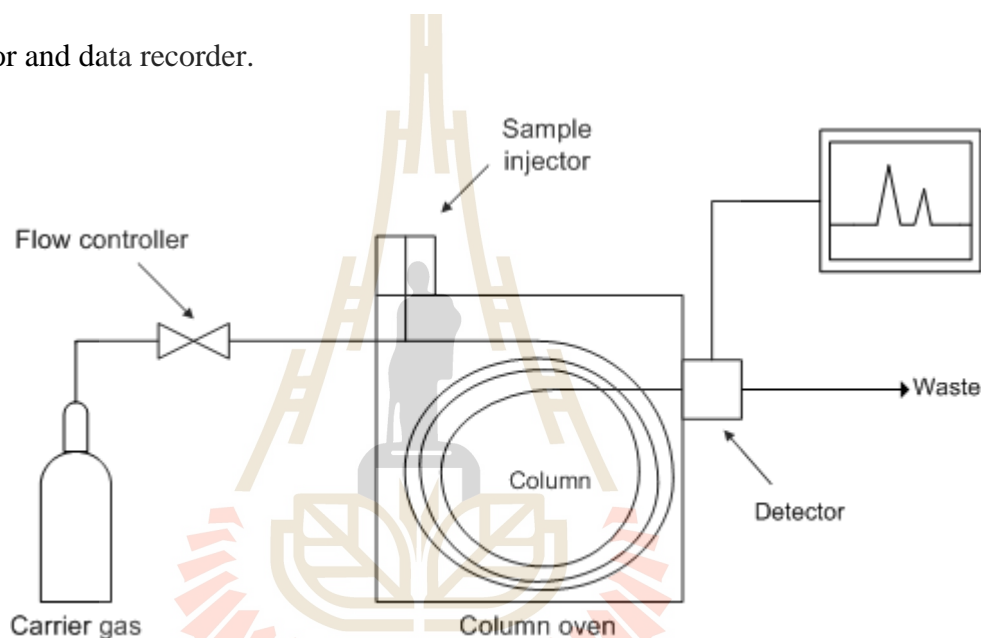
Figure 3.2 Block diagram of a gas chromatograph.

Carrier gas systems

The carrier gas or mobile phase, the main purpose of the carrier gas is to carry the constituents sample through the column and is to provide a suitable matrix for the detector to measure the sample components. The carrier gas it is inert and does not interact chemically with the sample. The carrier gases preferred for various detectors. For the thermal conductivity detector usually helium is the most popular. With the flame ionization detector, either nitrogen or helium may be used. Nitrogen provides slightly more sensitivity, but a slower analysis, than helium. For theelectron capture detector, very dry, oxygen-free nitrogen is recommended.

Injection systems

In gas chromatrography, the sample must be introduced into the analysis system in the from of a vapor. Vaporization can be achieved either during or after introduction of the sample.Liquid sample can be injected into the gaschromatograph by mean of a microliter syringe, while solid samples must be dissolved prior to injection, The purpose of injection systems is to allow thw insertion of a sample into a vapolirization chamber of the gas chromatrograph in a repeatable and reproducible manner. The sample must be introduced as a vapor in a smallest possible volume and a minimum of time without decomposition or fractionation occurring.

Capillary columns

The GC column is the core of the system. These consist of fused silica (silicon dioxide), alkali glass or borate glass. It is coated with a stationary phase which greatly influences the separation of the compounds. The structure of stationary phase affects the amount of time the compounds take to move through the column. Typical stationary phase are large molecular weight polysiloxanes, polyethylene glycols or polyesters polymer of 0.1 - 2.5 micrometer flim thicknesses. Column are available in many stationary phase sizes. A typical capillary column is 15 to 60 meter in length and 0.25 to o.32 mm ID.

Oven

The column oven should be free from the influence of changing ambient temperatures and have a well designed and adequate air flow system to maintain good temperatures control of the column. In most designs the air is blown past the heating coils, then through the baffles that comprise the inner wall of the oven, past the column, and back to the blower to be reheated and recirculated. For temperature programming it is desirable to have heat - up rates 0.25 °C/min to 10 °C/min. Heating

from ambient to 400 °C within 40 min, with cooling to 100 °C in 3 min, are the usual
working requirements.

Detectors

A detector senses the effluents from the column and provides a record of the
chromatograph in the from of a chromatogram. The detector signals are proportionate
to the quantity of each solute (analyte) making possible quantitative analysis.

Flame ionization detector (FID): The FID is the most widely used GC
detector, and is an example of the ionization detectors invented specifically for GC.
The column effluent is burned in a small air/hydrogen flame producing some ions in
the process. These ions are collected and from a small current that becomes the signal.
The FID responds to compounds that yield electrically charged species on combustion
in a hydrogen/air flame, the free-radical reaction being

$$CH + O \rightarrow CHO^+ + e^-$$
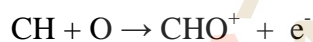
These charged species, under the influence of an electric field, are captured on a
collecting electrode and measured by an electrometer, whose output amplified. The
field of application of the FID is very large, as it responds to almost all organic
compounds.

Data recorders

The data recorder plots the signal from the detector over time. This plot is
called a chromatogram. The retention time, which is when the component elutes from
the GC system, is qualitatively indicative of the type of compound. The data recorder
also has an integrator component to calculate the area under the peaks or the height of
the peak. The area or height is indicative of the amount of each component.

3.4.6 Inductively Coupled Plasma Mass Spectrometry (ICP-MS)

Inductively coupled plasma mass spectrometry or ICP-MS is an analytical technique used for elemental determinations. The technique was commercially introduced in 1983 and has gained general acceptance in many types of laboratories. Geochemical analysis labs were early adopters of ICP-MS technology because of its superior detection capabilities, particularly for the rare-earth elements. ICP-MS has many advantages over other elemental analysis techniques such as atomic absorption and optical emission spectrometry, including ICP Atomic Emission Spectroscopy (ICP-AES), including: detection limits for most elements equal to or better than those obtained by graphite furnace atomic absorption spectroscopy (GFAAS). Higher throughput than GFAAS. The ability to handle both simple and complex matrices with a minimum of matrix interferences due to the high-temperature of the ICP source. Superior detection capability to ICP-AES with the same sample throughput and the ability to obtain isotopic information an ICP-MS combines a high-temperature ICP (Inductively Coupled Plasma) source with a mass spectrometer. The ICP source converts the atoms of the elements in the sample to ions. These ions are then separated and detected by the mass spectrometer. Argon gas flows inside the concentric channels of the ICP torch. The RF load coil is connected to a radio-frequency (RF) generator. As power is supplied to the load coil from the generator, oscillating electric and magnetic fields are established at the end of the torch. When a spark is applied to the argon flowing through the ICP torch, electrons are stripped off of the argon atoms, forming argon ions. These ions are caught in the oscillating fields and collide with other argon atoms, forming an argon discharge or plasma. The sample is typically introduced into the ICP plasma as an aerosol, either by aspirating a liquid or dissolved solid sample into a nebulizer or using a laser to directly convert solid samples into an aerosol. Once the sample aerosol is introduced into the ICP

torch, it is completely desolvated and the elements in the aerosol are converted first into gaseous atoms and then ionized towards the end of the plasma.
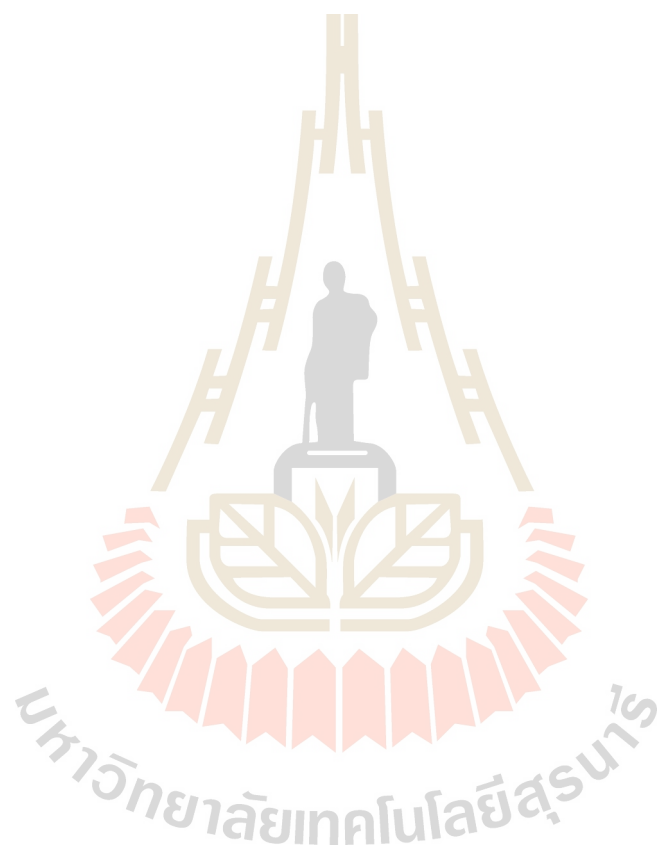
CHAPTER IV

RESULTS AND DISCUSSION

In this chapter, the analytical result of starting materials and the result for the synthesis of analcime and cancrinite were firstly discussed. Secondly, the result for synthesis of zeolite NaA and zeolite NaX and modified zeolite NaA and NaX with cations were considered. Finally, the results of water removal from ethanol solutions were discussed.

4.1 Characterization of kaolin and diatomite

Kaolin and diatomite used as the starting material in this study were characterized by using powder XRD and XRF to determine the phase and chemical compositions. FT-IR were also used to confirm the characteristic of samples. In figure 4.1, the XRD pattern showed the characteristic peaks of kaolin at $2\theta = 13$ and 25 (Carolina et al., 2002 and Marek et al., 2010) and an amorphous broad band at $2\theta = 20$ - 22 of diatomite (Figure 4.2) (Nezahat, İsmail and İlknur, 2010).

Table 4.1 shows the chemical compositions of the raw kaolin and diatomite which were determined by the wavelength dispersive XRF. The main chemical compositions of kaolin and diatomite were expressed as percent oxide by weight as follows for kaolin: SiO_2, 62.37%, Al_2O_3, 31.98%, Fe_2O_3, 1.34%, K_2O 1.65%, and 2.31% of TiO_2 and for diatomite: SiO_2, 71.51%, Al_2O_3, 11.09%, Fe_2O_3, 12.55%, K_2O 2.68%, and 1.05% of TiO_2. For acid activated diatomite, the chemical composition of SiO_2 was increased due to the leaching of Al_2O_3 and Fe_2O_3 by acid.

Table 4.1 The chemical compositions and Si/Al ratios of kaolin and diatomite samples determined by XRF.

Chemical content (% weight)	Kaolinite	Diatomite	DA
SiO_2	62.37	71.51	95.21
Al_2O_3	31.98	11.09	2.15
Fe_2O_3	1.34	12.58	0.43
K_2O	1.65	2.68	0.80
TiO_2	2.31	1.05	1.02
S	-	0.22	0.15
Si/Al ratio	1.65	5.46	26.98
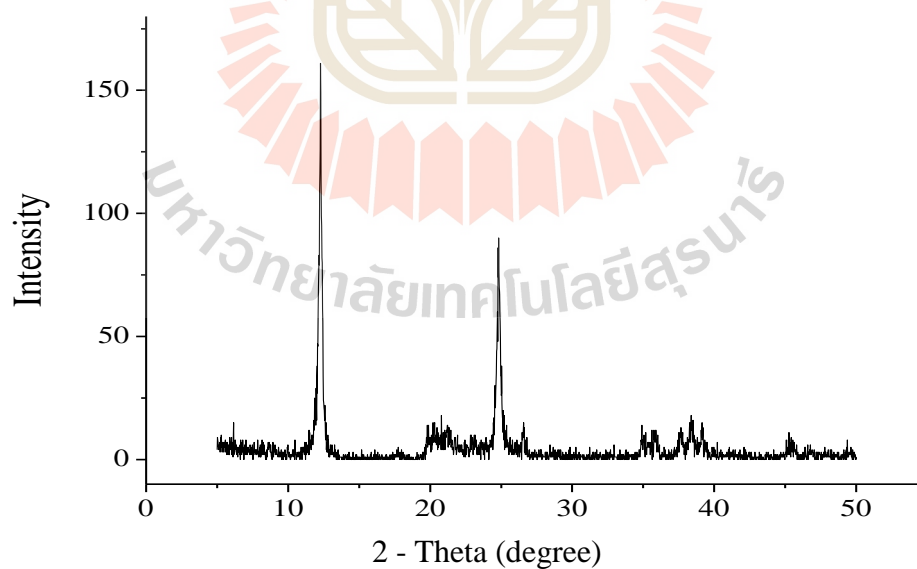
Figure 4.1 The XRD pattern of natural kaolin.
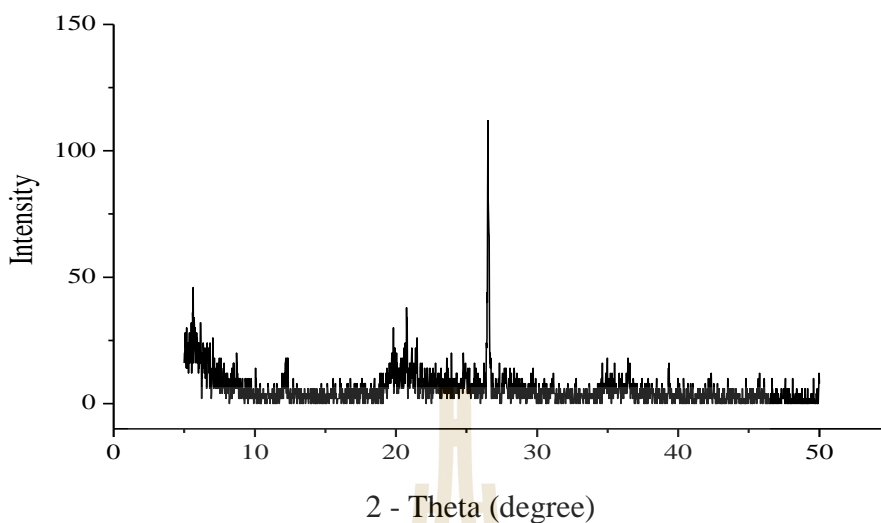
Figure 4.2 The XRD pattern of natural diatomite.

IR spectrum of natural kaolin sample was recorded in the mid infrared region as shown in figure 4.3. The vibrational bands of kaolin observed at 3696, 3671, 3653, and 3621 cm^{-1}. The three higher frequencies are assigned to O-H stretching modes of the three inner surface hydroxyl groups. The band at 3621 cm^{-1} is strong and sharp, assigned to the stretching mode of an inner hydroxyl group. The 3671 and 3653 cm^{-1} bands are weak and are described as the out-of-phase vibration (Breek, 1974 and Barrer, 1998). The intensity of the O-H stretching bands depends on the defect structure of the kaolinite. The band at 1031 cm^{-1} is attributed to the Si-O stretching vibration of the siloxane layer of kaolinite. Additional bands at around 789, 754, and 537 cm^{-1} should be associated to Al-O-Si vibrations of micas (Barrer,1998). Vibration of Al-OH appeared at around 913 and 935 cm^{-1}, and vibration of Si-O appeared at around 430, 470, 697, 1008, and 1114 cm^{-1} (Makó et al., 2006). The stretching and bending vibrations of adsorbed water forming H-bond in kaolin appeared at 3420 cm^{-1} and 1631 cm^{-1}, respectively.
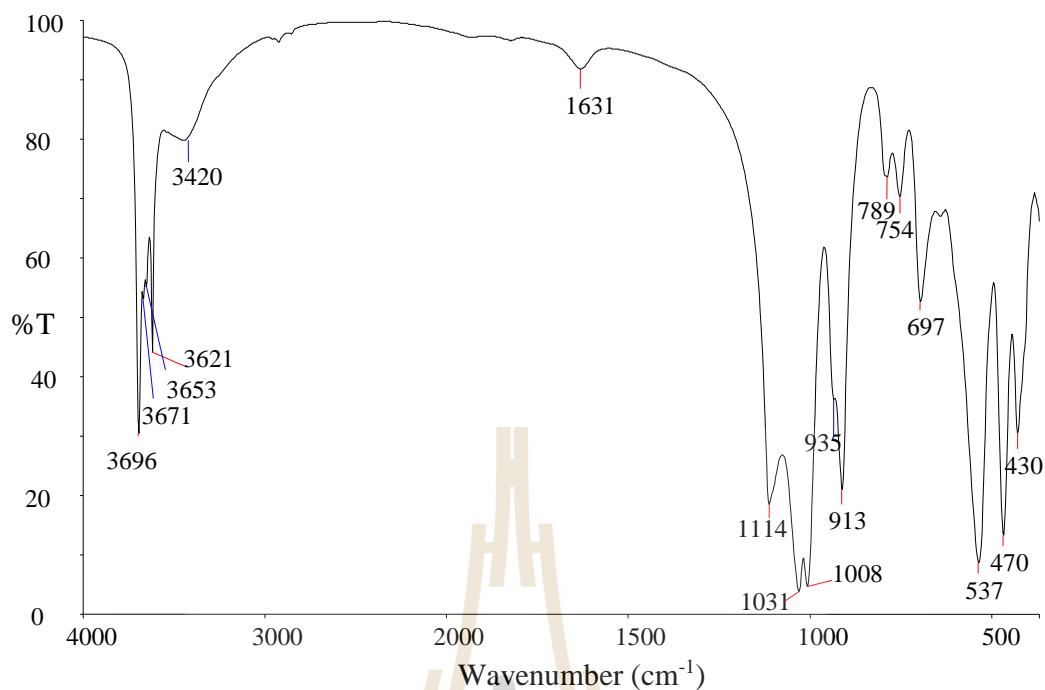
Figure 4.3 IR spectra of the natural kaolin.

The IR spectrum of natural diatomite was shown in Figure 4.4. The bands at 3698 and 3621 cm^{-1} (weak and narrow) are due to O-H stretching vibration of kaolinite, and the band at 3437 cm^{-1} and at 1634 cm^{-1} are assigned to O-H stretching and bending vibration of adsorbed water forming H-bonds, respectively. In the region of low wave numbers, there were up to 8 characteristic bands of natural diatomite, the bands at 1099 cm^{-1} (strong and broad) is mainly attributed to siloxane (Si-O-Si) stretching vibration of amorphous silica and at 1032 cm^{-1} is attributed to an impurity of kaolin. The bands at 798 and 781 cm^{-1} are correspond to an inter-tetrahedral Si-O-Si bending vibration, while 696 and 470 cm^{-1} bands were due to (O-Si-O) bending, and. 914 cm^{-1} (weak and broad) band may be due to Si-OH stretching and Al-Al-OH bending of kaolinite. The vibrational bands of kaolin and diatomite were summarized in Table 4.2.
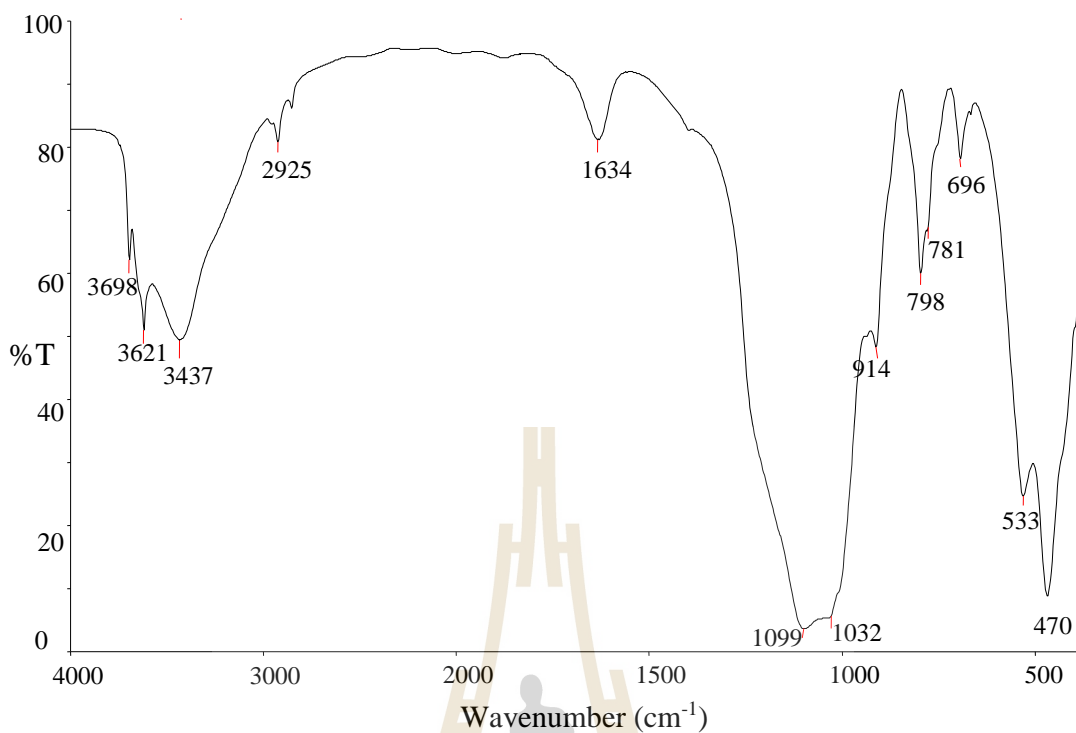
Figure 4.4 IR spectra of the natural diatomite.

Table 4.2 Identification of IR absorption bands to specific vibrations.

Vibrations	Wavenumber (cm^{-1})	
	kaolin	diatomite
O-H stretching of kaolinite	3696, 3671, 3653, 3621	3698, 3621
O-H stretching of water	3420	3437
H2O bending	1631	1634
Si-O-Si stretching	1032	1099, 1032
Si-OH stretching, Al-Al-OH bending (kaolinite)	913, 935	914
Intertetrahedral Si-O-Si bending	789, 754	798, 781
O-Si-O bending	697, 470, 430	696, 470
Si-O-Al bending	537	533

4.2 Characterization of analcime and cancrinite

The FT-IR, XRD and SEM were used to characterize the synthesized analcime and cancrinite. It was found that under the condition studied, the obtained solid phase was only pure phase of analcime and cancrinite with high percentage of crystallinity.

The XRD patterns show only pure phase of analcime and cancrinite (Figures 4.5 and 4.6). The phase identifications of different crystalline phases were realized by using diffraction pattern files provided by Joint Committee on Powder Diffraction Standards (JCPDS) and the verified syntheses of zeolitic materials (Robson, 2001). All of the samples showed clear diffraction peaks of analcime and cancrinite matching that of their literature values.
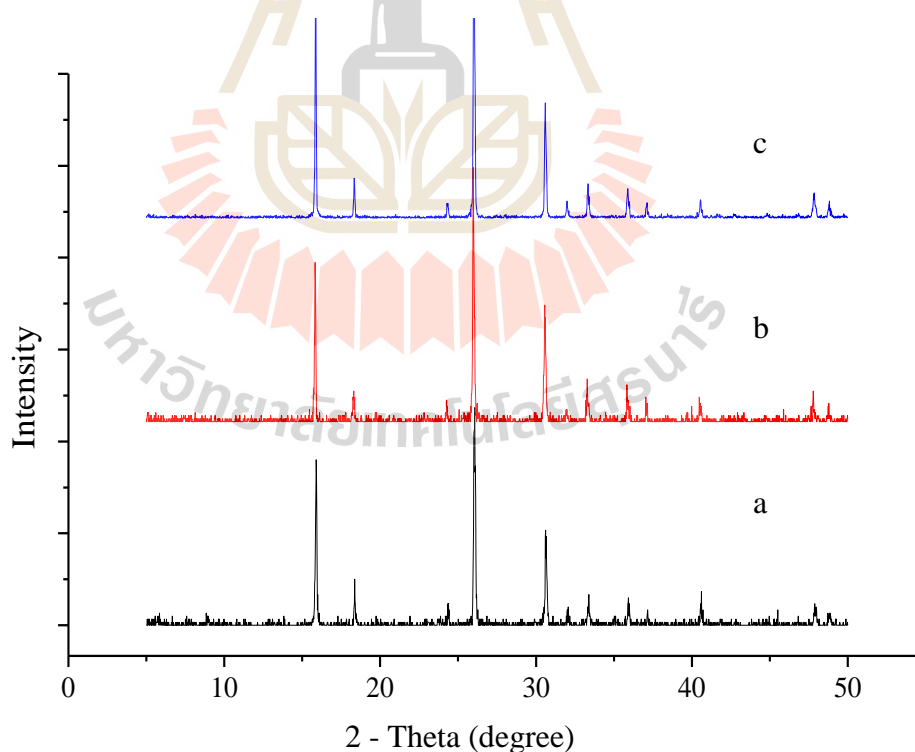
Figure 4.5 The XRD pattern of analcime from DA (a), DA-900 (b), and DA-1100 (c).
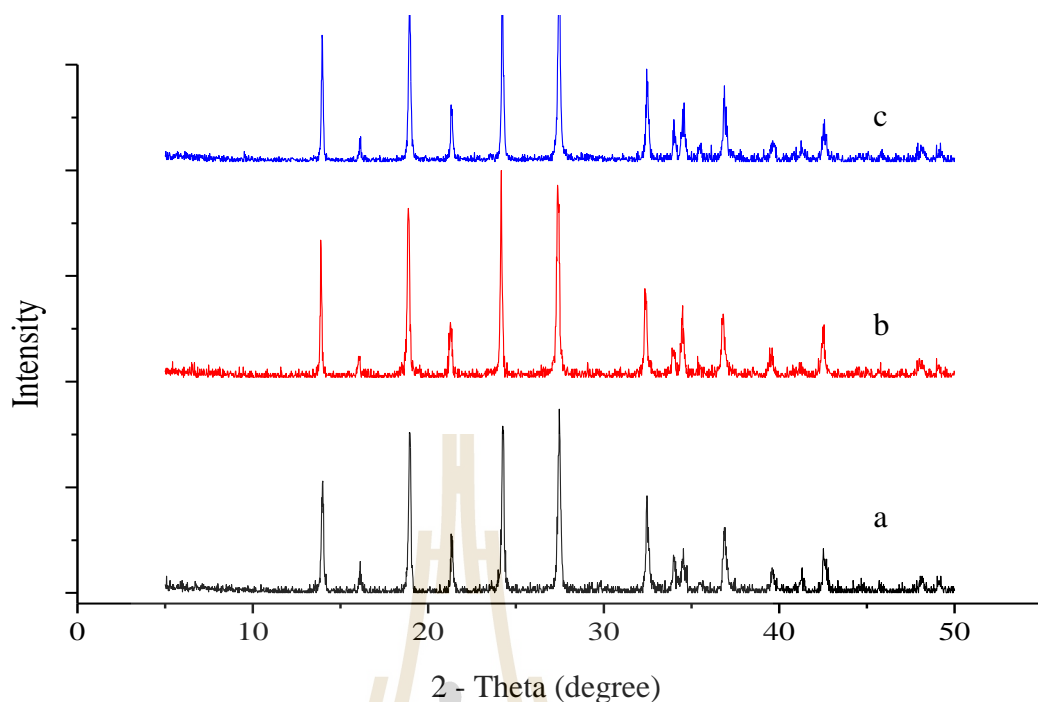
Figure 4.6 The XRD pattern of cancrinite from DA (a), DA-900 (b), and DA-1100 (c).

From the XRD patterns, each of analcime and cancrinite peaks started to appear gradually. Similar results were obtained for all starting materials. From the XRD results, natural diatomite material not calcined gave the lowest of yield because of the high concentration of impurity phase and the presence of high SiOH groups.

The SiOH groups make it less active towards analcime and cancrinite synthesis. The zeolites obtained from calcined diatomite samples at various temperature are higher than analcime and cancrinite obtained from natural diatomite material not calcined. Because of the high calcination temperature, the SiOH groups are almost eliminate in the dehydroxylation process (Halimaton et al., 1997) and the smaller particle size (higher surface area) favours contact between the reactants and decreases diffusion time (Antonucci, Crisafulli, Giordano, and Burriesci, 1985). Considering the sodium zeolites products started to appear gradually from natural diatomite treated with hot 6M H_2SO_4 material, calcined at 900 °C, and calcined at

1000 °C. It is cleared from the ^{29}Si MAS NMR spectra that the starting materials contain different amount of Q^2, Q^3 (total), Q^4 (total) species. The starting materials with higher Q^4 ($[Si(OSi)_4]$) content achieve a higher conversion in the zeolitization process. In addition, not only the Q^4 contents of starting material but also the particle size, the impurity phase and $Al(OH)_3$ can affect the zeolite synthesis (Chaisena and Rangsriwatananon, 2005).

IR spectrum of analcime and cancrinite heated for 24 hours at 110 °C, in a KBr matrix was recorded in the range of 4000 cm^{-1} to 370 cm^{-1} (Figures 4.7 and 4.8). Analcime synthesized from diatomite treated with acid showed an absorption band at 3622 cm^{-1} and a strong water absorption band at 3460 cm^{-1} and 1639 cm^{-1}. The absorption band at 3622 cm^{-1} is assumed to be a band of Si-OH. The stretching vibration band of bound water in analcime at 3460 cm^{-1} shifts to a lower wave number at 3455 cm^{-1} and 3452 cm^{-1} when using analcime synthesized from DA-900 and DA-1100, respectively. The absorption spectra of all obtained zeolites were in total accordance with the different absorption peaks given by Flanigen, Khatami and Szymanski, 1971; Breck, 1974. Analcime showed absorption bands at 1108, 1038, 1006, 961, 757, 682, 624, 567, 503, 459, 428, and 387 cm^{-1} and cancrinite showed absorption bands at 1113, 985, 736, 708, 666, 567, 463, and 435 cm^{-1}. Vibrations in a region of TO$_4$ tetrahedral (T = Si or Al) units of zeolite, bands at about 1,024 cm^{-1}, 736 cm^{-1}, 621 cm^{-1} and 444 - 460 cm^{-1}, are assigned to asymmetric, symmetric stretching, double ring and T-O bending vibrations, respectively (Breck, 1974). However, infrared assignments of vibration frameworks of analcime and cancrinite were shown in Table 4.3.

Table 4.3 Infrared assignments of vibrational frameworks of analcime and cancrinite.

Zeolite	Asymmetric stretching	Symmetric stretching	Double ring	T-O bending
Analcime	1024	736, 687	621	444
Cancrinite	1011, 969	680	625, 567	460
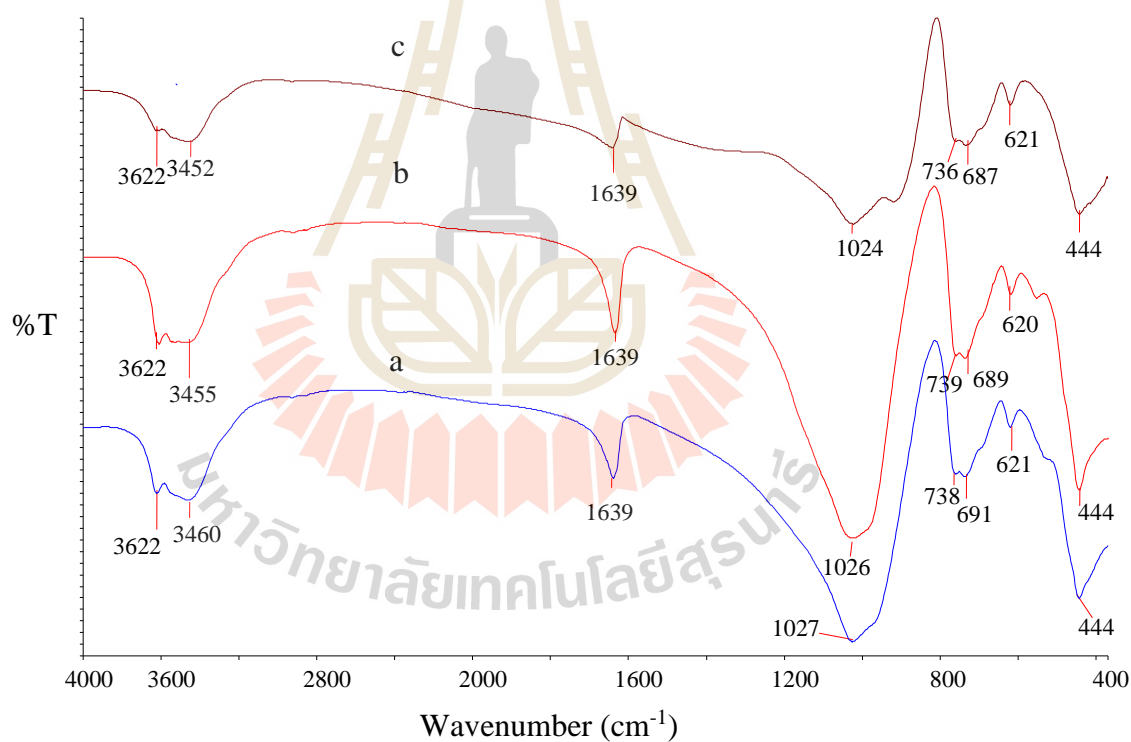
Figure 4.7 IR spectra of the analcime from DA (a), DA-900 (b), and DA-1100 (c).
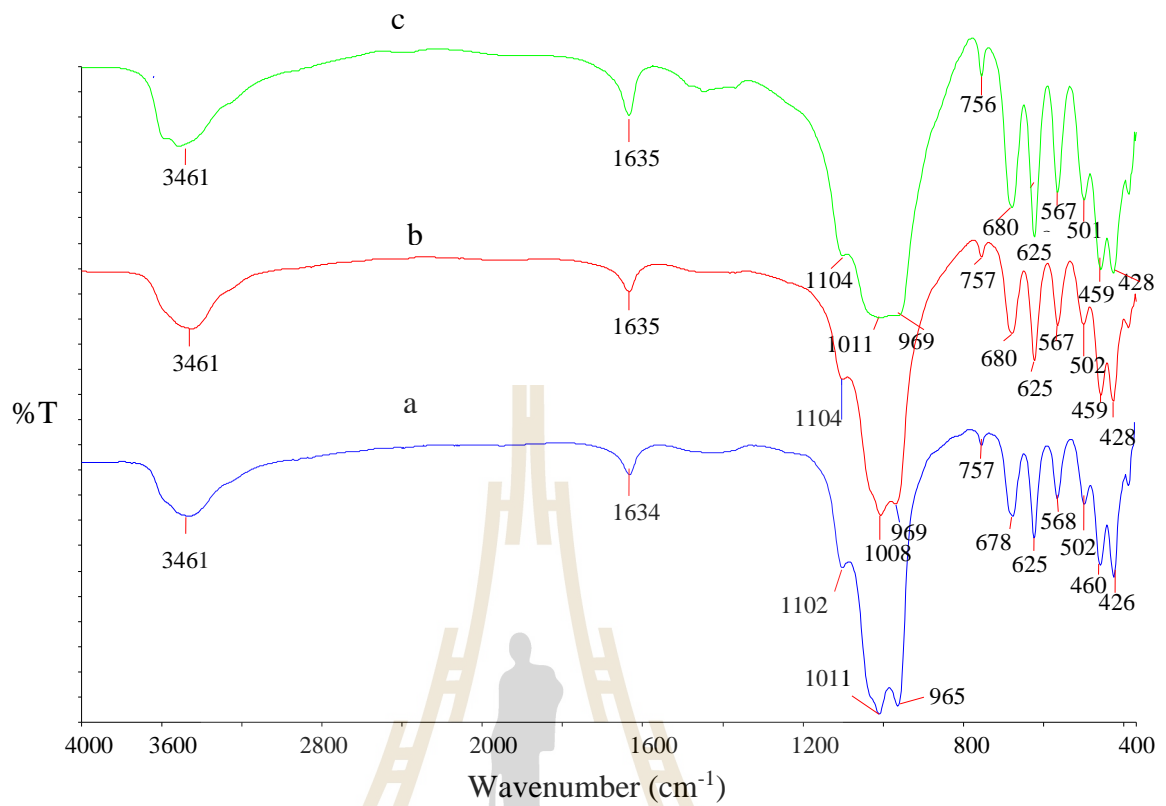
Figure 4.8 IR spectra of the cancrinite from DA (a), DA-900 (b), and DA-1100 (c).

The morphologies of analcime and cancrinite were shown in Figures 4.9 and 4.10, respectively. Analcime had icosahedral shape and the cancrinite appeared in fractal shape comprised of extended bars.
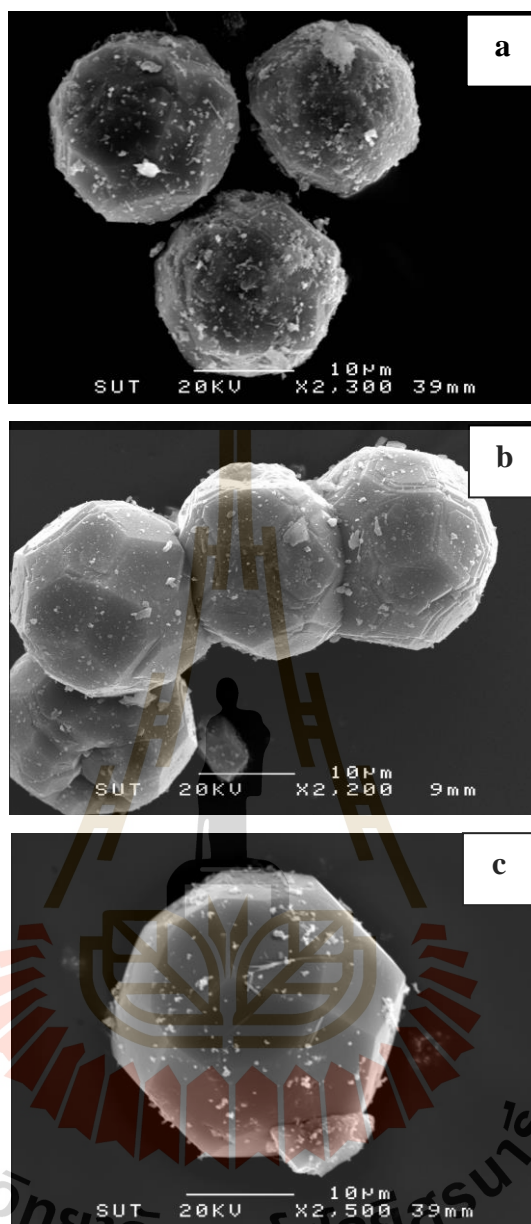
Figure 4.9 SEM photographs of analcime crystals prepared from DA (a), DA-900 (b),
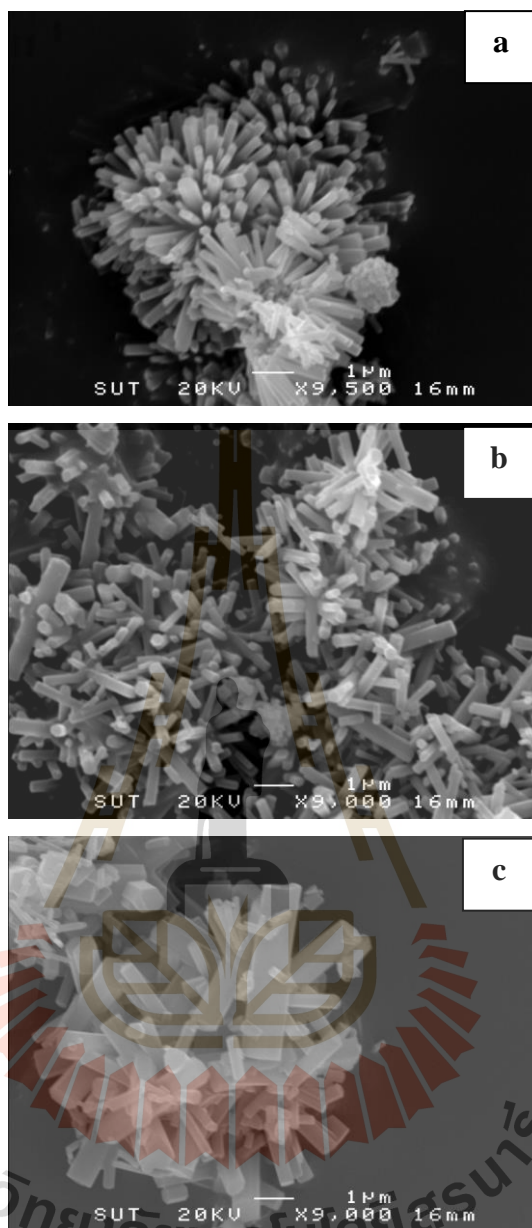
and DA-1100 (c).

Figure 4.10 SEM photographs of cancrinite crystals prepared from DA (a), DA-900

(b), and DA-1100 (c).

4.3 Characterization of zeolite NaA and zeolite NaX and zeolite NaA and zeolite NaX modified with cation

Figures 4.11 and 4.12 show XRD patterns of zeolite NaA and zeolite NaX. Only pure phase of zeolite and high crystallinity were observed, indicating that zeolite NaA and zeolite NaX were successfully synthesized from kaolin. The phase identification was performed by comparing the observed powder patterns with the verified syntheses of zeolitic materials (Robson, 2001) and JCPDS database. All strong XRD patterns of zeolite NaA and zeolite NaX from synthesized matching that of their literature values. The XRD patterns of zeolite NaA and zeolite NaX as well as their modifications with various cations are shown in Figures 4.13 and 4.14

After modification with cations, the percentage of crystallinity of zeolite NaA and zeolite NaX was decreased to 20 - 60% (see Table 4.4) depending on type of zeolites and obviously limited by metal ion charge (Paul and Karl, 1974). It is clearly seen that the framework of zeolite NaA was more destroyed than that of zeolite NaX due to the pore size of zeolite NaA was smaller than that of zeolite NaX and the framework was significantly destroyed by Co^{2+} comparing to the other cations. It may result from its higher charge density thus increasing its effective size or its hydrodynamic radius. But the percentage of crystallinity for both zeolites modified with Cu^{2+} unable calculated because the peaks of zeolites were disappearing. Because zeolites can produces hydroxide ions in water cause limited hydrolysis of the more loosely bound cations (Afzal et al., 2000). In solution occur $Cu(OH)_2$ affect zeolites framworks were destroyed.
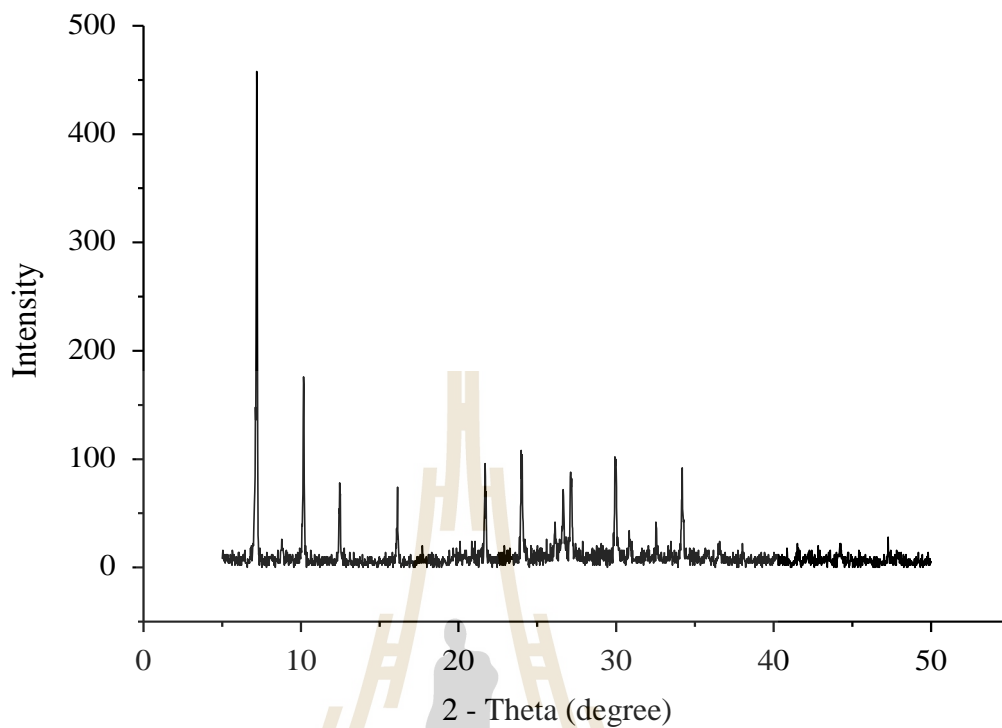
Figure 4.11 The XRD pattern of synthesized zeolite NaA.
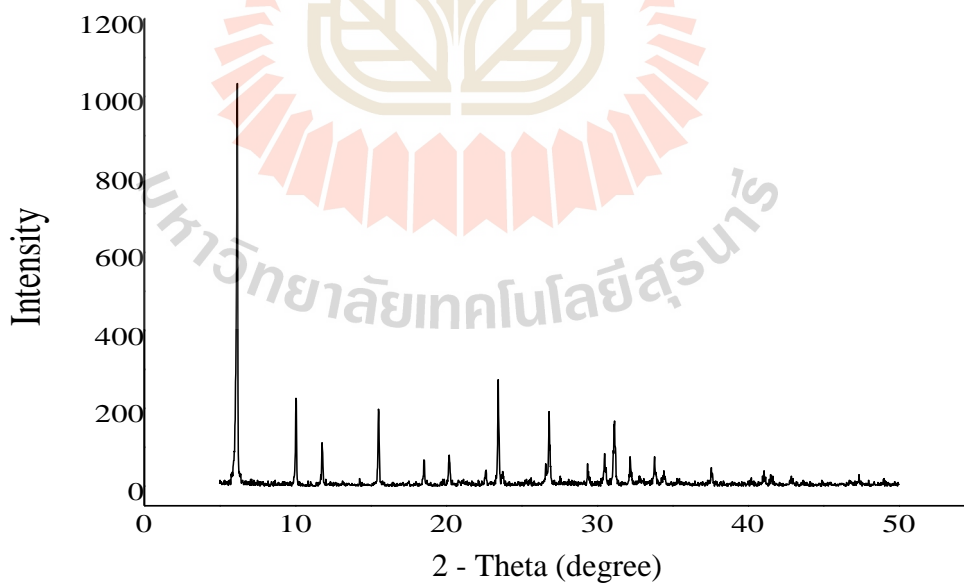
Figure 4.12 The XRD pattern of synthesized zeolite NaX.
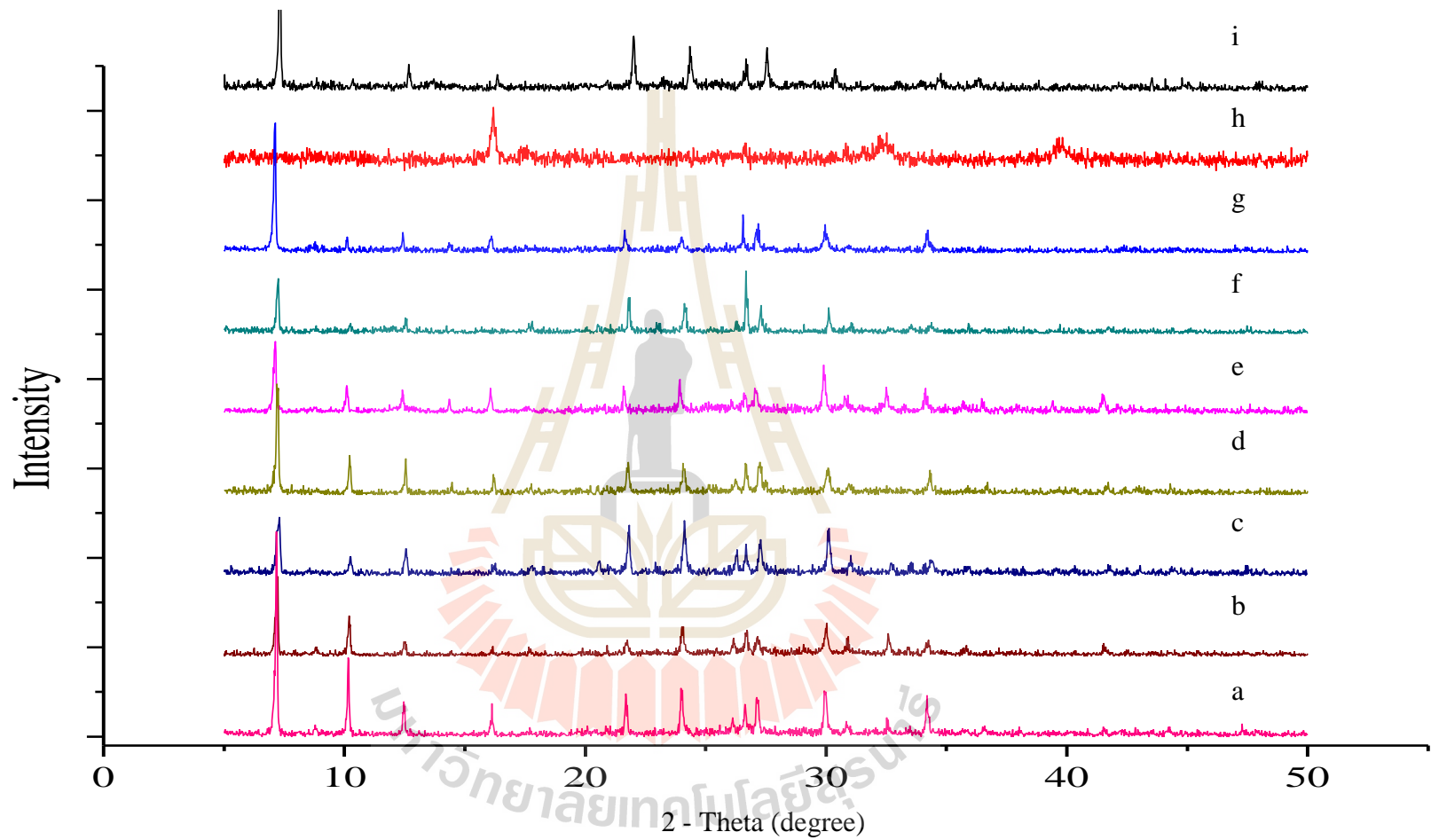
Figure 4.13 The XRD patterns of zeolite NaA (a) and zeolite NaA modified with K^+ (b) , Mg^{2+} (c) , Ca^{2+} (d) , Sr^{2+} (e), Co^{2+} (f), Ni^{2+} (g) , Cu^{2+} (h), and Zn^{2+} (i).
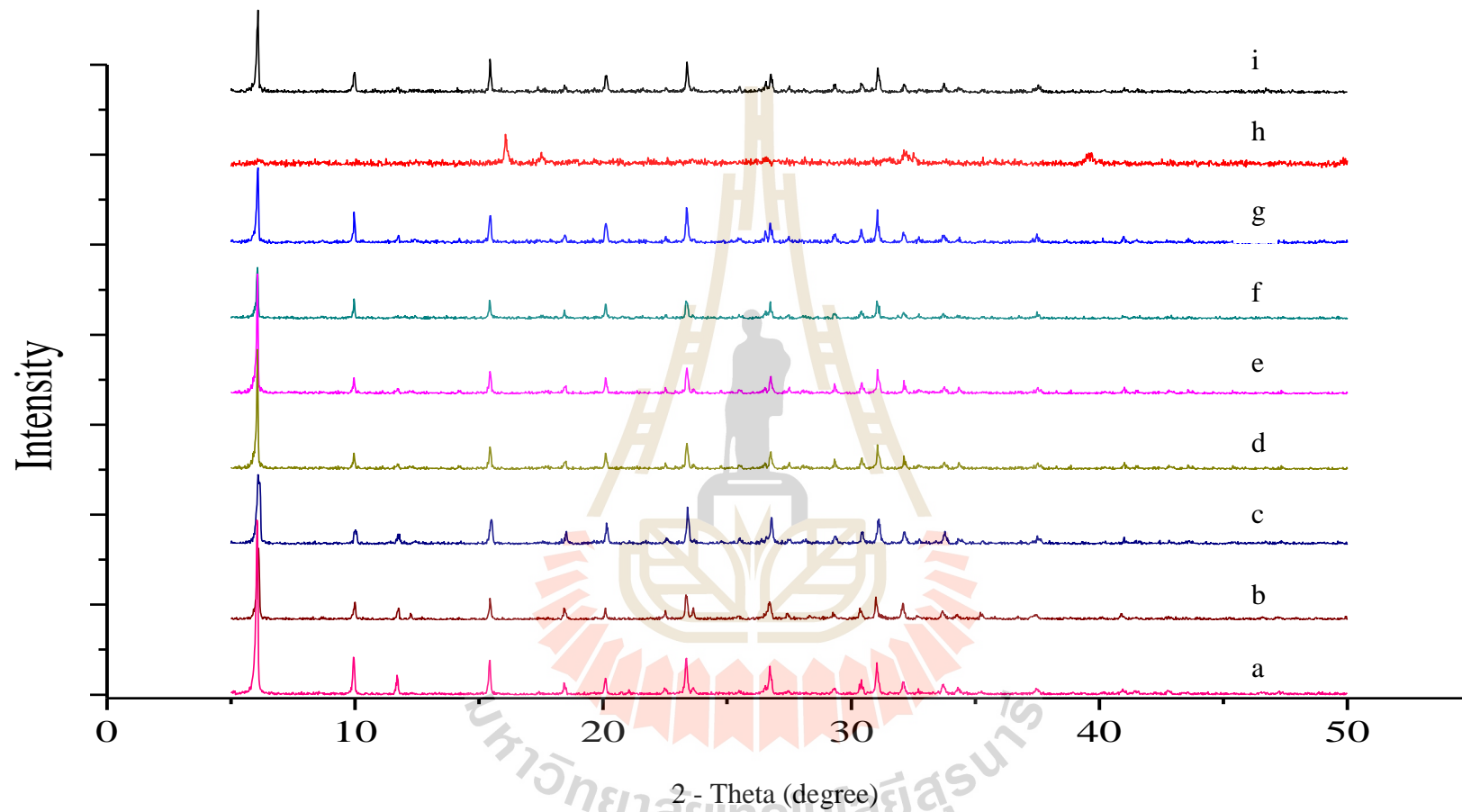
Figure 4.14 The XRD patterns of zeolite NaX (a) and zeolite NaX modified with K^+ (b) , Mg^{2+} (c) , Ca^{2+} (d) , Sr^{2+} (e), Co^{2+} (f), Ni^{2+} (g) , Cu^{2+} (h), and Zn^{2+}(i).

As stated earlier the positions of the atoms in the unit cell affect the intensites. More generally, the intensity of a diffracted beam is changed, not necessarily to zero, by any change in atomic positions, and conversely, atomic positions can be determined only by observations of diffracted intensites. To establish an exact relation between atom position and intensity is the main purpose of this. The problem is complex because of the many variables involved, and the relationship must be developed step by step: first by considering how x - rays are scattered by a single electron, then by an atom, and finolly by all the atoms in the unit cell. These results are applied next to the powder method of x - ray diffraction and, to obtain an expression for the intensity of a powder pattern line, a number of factor which affect the way in which a crystalline powder diffracts x - ray must be included.

When a beam of X-radiation falls onto an adsorber, a number of different processes may occur. In this exchample, a monochromatic beam of radiation of wavelength λ and intensity I_0 s incident on an absorber of thickness t and density ρ. A certain portion, I, of the radiation may pass through the absorber. Where this happens the wavelength of the tranmitted beam is unchanged and the intensity of this transmitted beam $I(\lambda)$ is given by

$$I(\lambda) = I_0(\lambda) \exp\left[-\left(\frac{\mu}{\rho}\right)\rho t\right],$$

where $\dfrac{\mu}{\rho}$ is the mass attenaution coefficient of the absorber for the wavelength λ and the density ρ. This equation is very general and is called the mass-absorption law. The value of the X-ray mass attenuation coefficent $\dfrac{\mu}{\rho}$ in equation is a function both of the photoelectric adsorption and the scatter (Jenkins and Snyder, 1996). From the

equation above mass absorption coefficients is not affected to a decrease in percentage crystallinity of zeolites after their modified with cations.

Table 4.4 Percentage crystallinity of zeolites and their modified with cations and mass absorption coefficients of cations.

	% Crystallinity		Mass absorption coefficients (cm^2/gm) (Cullity and Stock, 2001)
Cations	Zeolite NaA	Zeolite NaX	
-	100	100	-
K^+	60.2	67.4	148.4
Mg^{2+}	78.0	88.4	40.88
Ca^{2+}	76.7	65.3	171.4
Sr^{2+}	56.8	60.6	115.3
Co^{2+}	45.2	41.9	338.6
Ni^{2+}	56.9	71.4	48.83
Cu^{2+}	-	-	51.54
Zn^{2+}	72.2	58.18	59.51

Figure 4.15 shows IR spectra of zeolite NaA and zeolite NaA modified with various cations. The band at 465 cm^{-1} is related to Si-O and four coordinated Al-O bending. The band at 555 cm^{-1} associated with the double four membered rings is the characteristic of zeolite A (Rocha and Klimiwski, 1991). The band at 1002 cm^{-1} is identified as asymmetric stretching of Si-O or Al-O bonds. The bands around 3437 - 3428 cm^{-1} are attributed to O-H of water forming hydrogen bond. These bands are strongly shifted to lower wave number for cation modified zeolites comparing to unmodified zeolites. It indicates that the water molecules encountering cations (Sr^{2+}, Mg^{2+}, Co^{2+}, and Ni^{2+}) can form stronger H-bond with the neighboring water molecules

than those to Na^+ and K^+. The band of water in zeolite containing Co^{2+} located at the lowest wavenumber indicating that water has the strongest H-bond. Therefore, Co^{2+} modified zeolite NaA can adsorb water more than zeolites modified with the others.

Figure 4.16 shows IR spectra of zeolite NaX and zeolite NaX modified with various cations. The band at 565 cm^{-1} is attributed to double six rings (D6R) which is related to a faujasite structure (Breek, 1974 and Barrer, 1998). The strongest vibration at 991 cm^{-1} is assigned to a T-O-T (T = Si or Al) stretch and the stretching modes involving mainly the tetrahedral atoms are assigned in the region at 758 cm^{-1} and 682 cm^{-1}. After modified with Mg^{2+}, Co^{2+}, and Ni^{2+} it was found that an additional peak at 920 cm^{-1} due to vibration of Al-OH. For water vibration bands in zeolite NaX around 3496 - 3430 cm^{-1}, the spectra are similar to those in zeolite NaA. Therefore, Co^{2+} modified zeolite zeolite NaX can adsorb more water than zeolites modified with the other cations.

Both zeolite NaA and NaX showed the band around 3411 - 3460 cm^{-1} are attributed to O-H of water forming hydrogen bond. These bands are largely broad and strongly shifted to lower wave number for cation modified zeolites comparing to unmodified zeolites. It can explained about stronger H-bond with the neighboring water molecules for the water molecules encountering cations with transition metal (Co^{2+}, Ni^{2+}, Cu^{2+}, and Zn^{2+}) and more than main metal (Ca^{2+}, Mg^{2+}, and K^+). In the case of Cu^{2+} into zeolite NaA and zeolite NaX these band shows split to two peaks located at 3445 and 3361 cm^{-1}. The narrow band at 3445 cm^{-1} and one wider band at 3361 cm^{-1} assigned to free OH groups and hydrogen bonded OH groups, respectively (Jhon et al., 2011 and Henrist et al., 2003). The band of water in zeolite containing Co^{2+} located at the lowest wavenumber indicating that water has the strongest H-bond.

Therefore, Co^{2+} modified zeolite can adsorb water more than zeolites modified with the others cations.
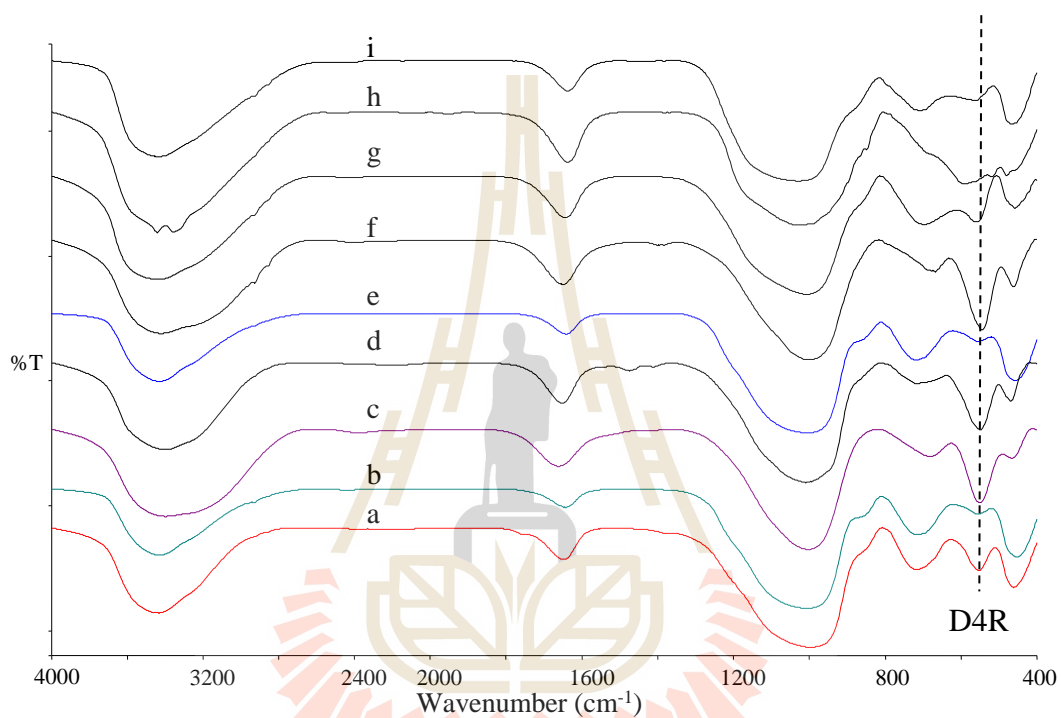
Figure 4.15 IR spectra of zeolite NaA (a) and zeolite NaA modified with K^+ (b), Mg^{2+} (c), Ca^{2+} (d), Sr^{2+} (e), Co^{2+} (f), Ni^{2+} (g), Cu^{2+} (h), and Zn^{2+}(i).
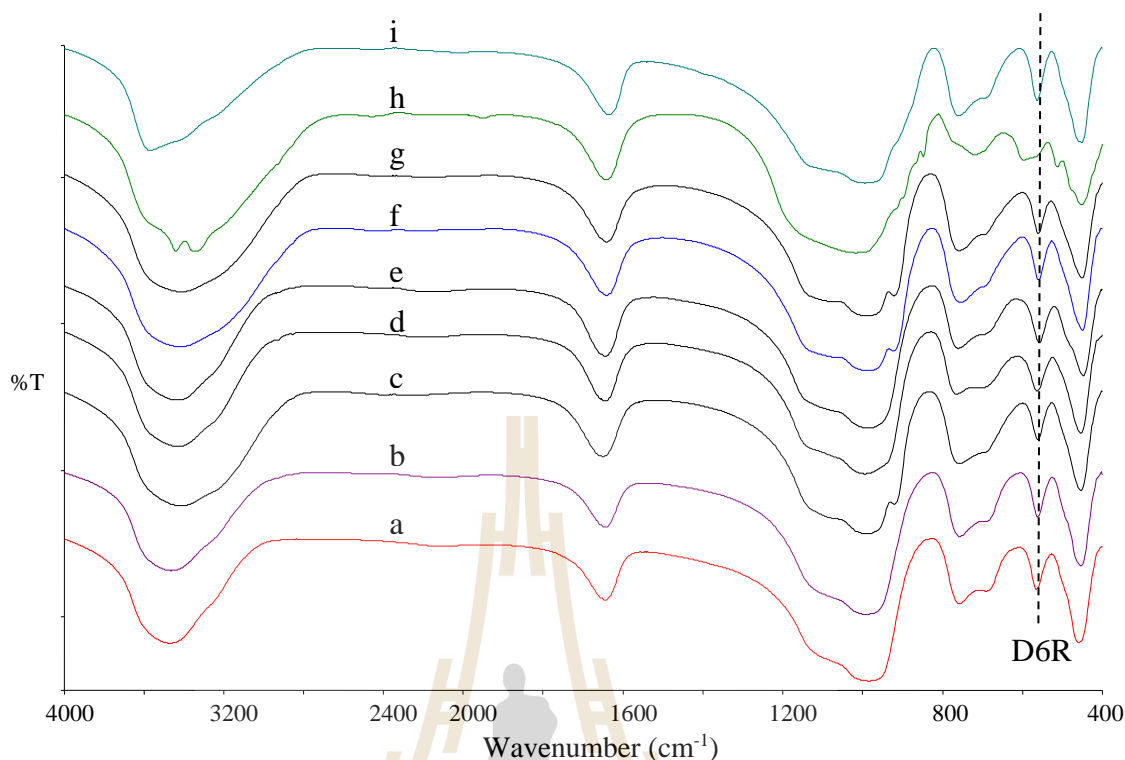
Figure 4.16 IR spectra of zeolite NaX (a) and zeolite NaX modified with K^+ (b),

Mg^{2+} (c), Ca^{2+} (d), Sr^{2+} (e), Co^{2+} (f), Ni^{2+} (g), Cu^{2+} (h), and Zn^{2+}(i).

4.4 Characterization by ICP-MS

The hydrophilic and hydrophobic nature and stability of zeolites can be tuned by changing the Si/Al ratio in the framework of the zeolites. The cation that balances the negative charge associated with framework aluninum ions creates an electrostatic field in the zeolite. Increase of Si/Al ratio of zeolite membranes can enhance its thermal and acid stability, though the hydrophilicity prooerties decrease (Oyama and Stagg-Williams, 2011). The Si/Al ratio of anacime more than zeolite NaX, zeolite NaA and cancrinite, respectively was show in Table 4.5, relationship to hydrophilic prooerties of cancrinite more than zeolite NaA, Zeolite NaX, and anacime, respectively

Table 4.5 The Si/Al ratios of analcime, cancrinite zeolite NaA and zeolite NaX determined by ICP-MS.

	Si/Al ratios
Analcime	1.98
Cancrinite	1.10
Zeolite NaA	1.18
Zeolite NaX	1.35

Cation contents in each zeolite were analyzed by ICP - MS. The results in Table 4.6 show an amount of cations loading in to zeolite NaA and zeolite NaX by ion exchange process and the mol ratio of Na : cations was shown in Table 4.7.

The mol ratio of Na^+ to Cu^{2+} on both zeolite NaA and NaX was higher than the other cations. It might be caused from that the structure frameworks was mostly destroyed which was indicated by XRD. Mol ratio of Na^+ to K^+, Mg^{2+}, Ca^{2+}, and Sr^{2+} on zeolite NaX more than zeolite NaA. This result can explain by ionic radius of cations K^+, Ca^{2+}, and Sr^{2+} more than Na^+ (Table 4.8) and pore size of zeolites NaX more than zeolite NaA.

In contrast, One mol of Na^+ to Co^{2+} and Ni^{2+} for zeolite NaA higher than zeolite NaX were indicated. The results agree with different Si/Al ratio because lower Si/Al ratio by the ratio of zeolite NaA rangs from 1.0 to 1.2 and zeolite NaX is between 1.0 and 1.5 influences to exchange capacity (Chang, 2000). Moreover, ionic radius of Co^{2+} (0.58Å) with Na^+ (0.99Å) near than Ni^{2+} (0.55Å) therefore Co^{2+} can exchange Na^+ on both zeolites more than Ni^{2+}.

Table 4.6 Cation contents in modified zeolite NaA and zeolite NaX.

	Cation content % (w/w)	
Cations	Zeolite NaA	Zeolite NaX
K^+	7.25	9.34
Mg^{2+}	3.75	3.32
Ca^{2+}	0.15	4.18
Sr^{2+}	14.40	17.76
Co^{2+}	12.50	10.23
Ni^{2+}	12.75	10.63
Cu^{2+}	25.48	24.43
Zn^{2+}	14.90	10.12

Table 4.7 Mole ratio of Na : cations.

	Mole ratio of Na : cations (mol)		Effective radius (Å)
Cations	Zeolite NaA	Zeolite NaX	
K^+	1: 1.53	1: 1.81	1.37
Mg^{2+}	1: 0.77	1: 0.84	0.57
Ca^{2+}	1: 0.01	1: 1.59	1.00
Sr^{2+}	1: 1.15	1: 3.63	1.18
Co^{2+}	1: 1.93	1: 1.55	0.58
Ni^{2+}	1: 1.75	1: 1.28	0.55
Cu^{2+}	1: 14.41	1: 9.32	0.57
Zn^{2+}	1: 0.15	1: 1.25	0.60

4.5 Thermal analysis

The differential thermogravimetric curves (DTG) of water adsorbed on zeolites were shown in Figures 4.17 and 4.18. The endothermic peaks of dehydration on NaA and zeolite NaX appeared at 134 °C and 124 °C, respectively, indicating that the interaction of water bound on zeolite NaA is more stronger than that on zeolite NaX. After modified with cations (K^+, Ca^{2+}, Co^{2+}, Ni^{2+}, and Cu^{2+}) all the endothermic peaks were changed to higher temperature (162.81, 201.81, 170.81, and

169.99 °C, respectively). It revealed that the bound water interacts much more strongly with the other non-framework cations (K^+, Ca^{2+}, Co^{2+}, Ni^{2+}, and Cu^{2+}) because they have higher charge density than Na^+. When compared DTG curve of monovalent ion (K^+) at 149.39 °C with divalent ions (Ca^{2+}, Co^{2+}, Ni^{2+}, and Cu^{2+}), the endothermic peaks of water bound to divalent cations appeared at higher temperature (Figure 4.18). This result agrees with the results of hydration energy (Table 4.8).

Table 4.8 Ionic radius and hydration enthalpies of metal cations.

Ion	Radius ($\overset{\circ}{A}$)	ΔH_{hyd} (kJ mol^{-1})
Na^+	0.99	-405
K^+	1.37	-321
Mg^{2+}	0.57	-1922
Ca^{2+}	1.00	-1592
Sr^{2+}	1.18	-1443
Co^{2+}	0.58	-1996
Ni^{2+}	0.55	-2106
Cu^{2+}	0.57	-2100
Zn^{2+}	0.60	-2044
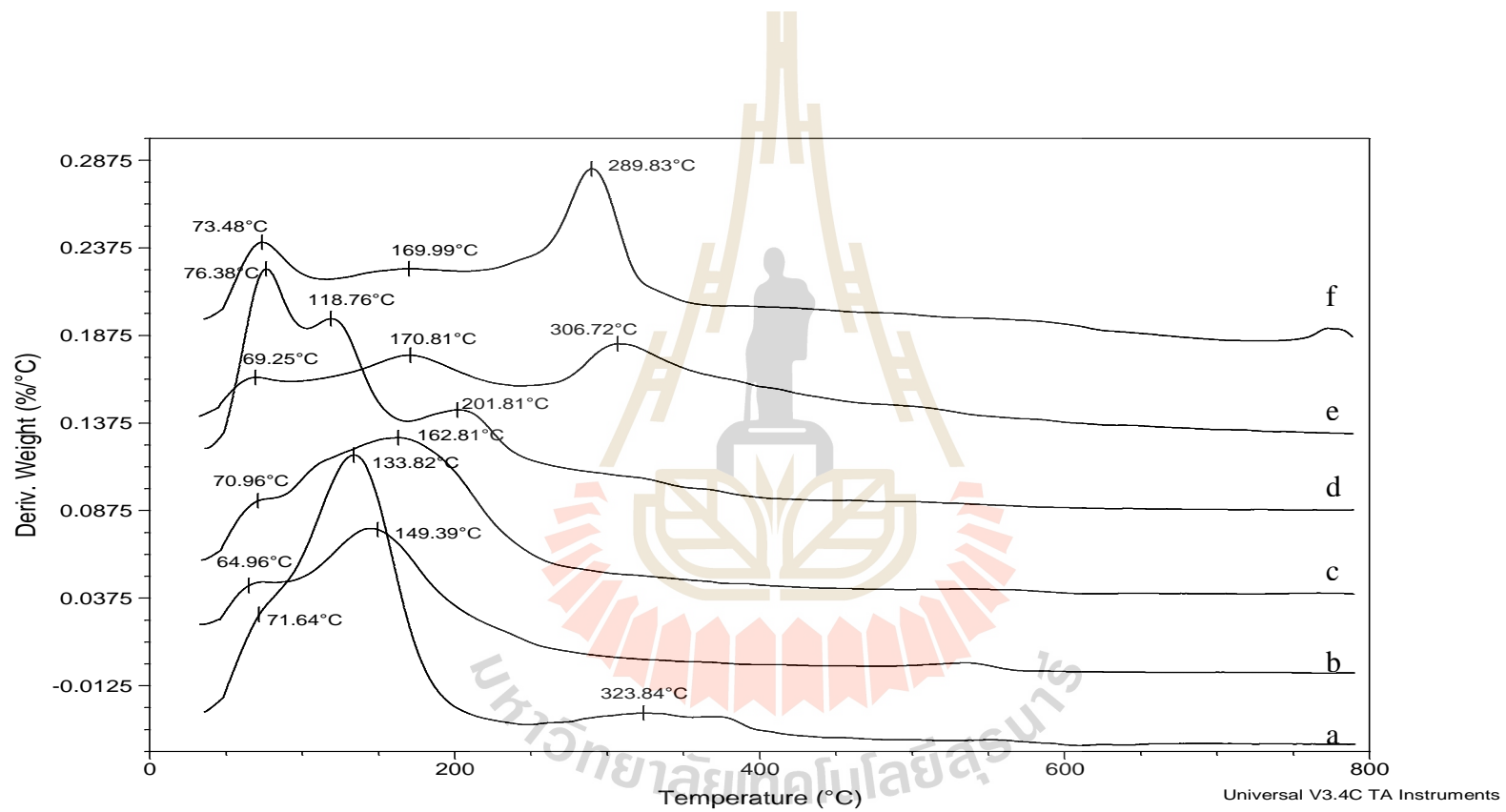
Figure 4.17 Differential thermogravimetric curves (DTG) of zeolite NaA (a), zeolite NaA modified with K^+ (b), Ca^{2+} (c), Co^{2+} (d), Ni^{2+} (e), and Cu^{2+}(f).
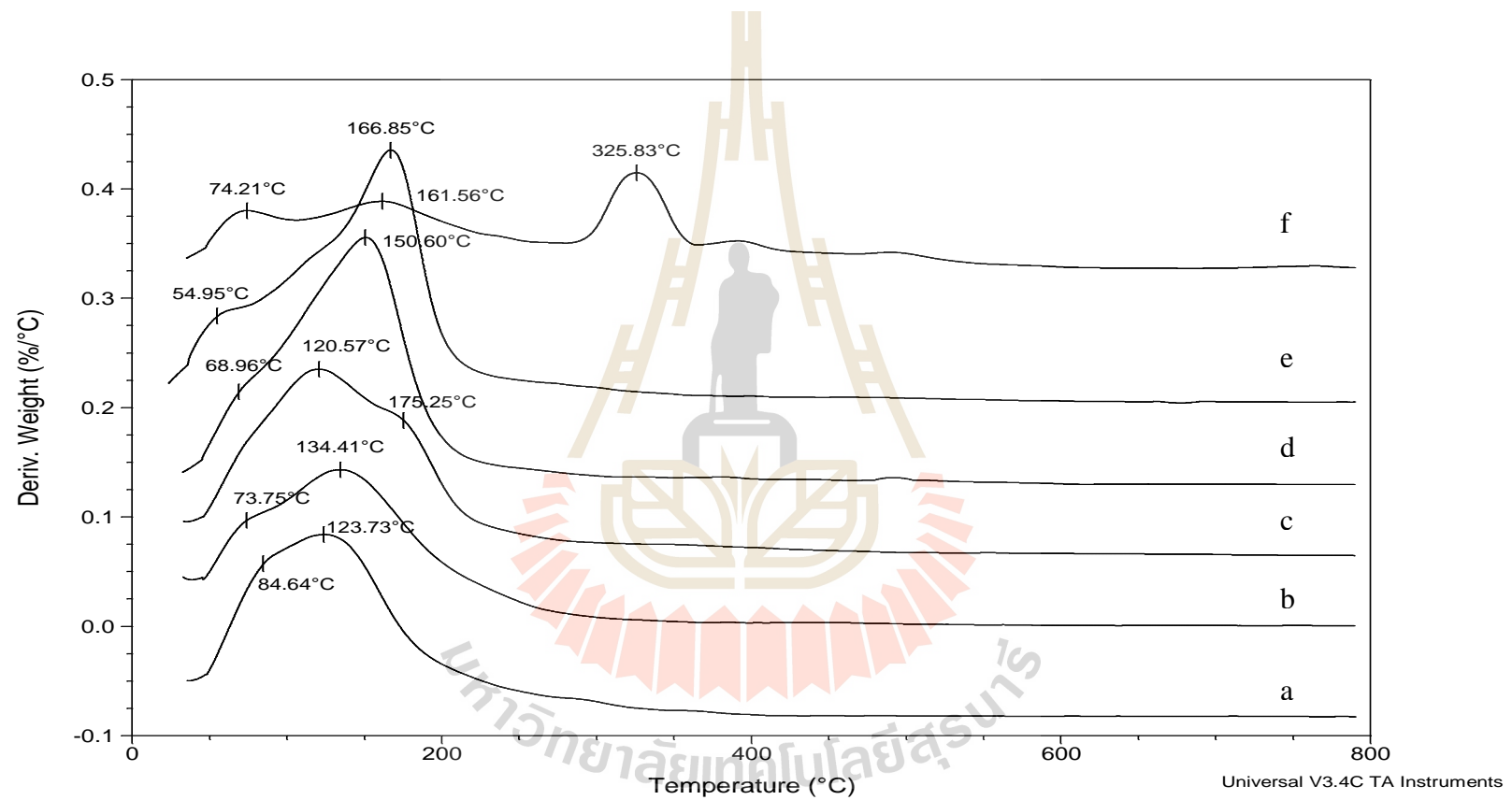
Figure 4.18 Differential thermogravimetric curves (DTG) of zeolite NaA (a), zeolite NaA modified with K^+ (b), Ca^{2+} (c),

Co^{2+} (d), Ni^{2+} (e), and Cu^{2+} (f).

4.6 Elimination of water from ethanol solution by zeolites

Tables 4.9 - 4.11 showed the concentrations of ethanol solution before and after adsorption with various adsorbents. The results showed that the concentration of ethanol solution was increased in all adsorbents. But modified zeolite NaA and zeolite NaX with Co^{2+} are much more capable to eliminate water compared to the other modified zeolites.

Analcime and cancrinite have a small pore size around 2-3 Å and a low CEC, small channels, and hence have a low potential application as either a molecular sieve or ion exchanger (Cox, Nugteren and Janssen-Jurkovičová, 2008). The concentration of ethanol solution was increased after adsorption with analcime and cancrinite up to 99.6 and 99.3%, respectively (see Table 4.9).

Since the trem zeolite in used for a large group of crystalline Al-Si phases, withvery different properties and applications, it should be clarified that the zeolitic materials it used as molecular sieves and ion exchangers. Zeolite A is a typical small-pore zeolite 4.1 Å (Čejka and Van Bekkum, 2005) with larg cavities (Oyama and Stagg-Williams, 2011). If the silica per alumina ratio of zeolite A is held at 2:1, in its sodium from the cross-sectional diameter is 0.41 nm, compared with a cavity diameter of 1.14 nm. This is why only linear organic molecules may enter the pores of zeolite A. Once inside the structure, molecules may react within the cavities to produce much larger intermediates/transition states. However, the final products must be small enough to allow them to exit from the zeolite. The pore system of zeolite A can be widened by removing some of the sodium ions normally present and replacing them with calcium ions. The result of this ion exchange is to increase the effective pore size to 0.5 nm conversely, if the sodium is replaced by potassium this is reduced to 0.3 nm,

allowing only water molecules into the cavities in the system. This alteration of the dimensions of pore systems by cations is termed the sentinel effect. The simplest explanation of why the replacement of sodium ions changes the diameter of the pores in zeolite A is that K^+ ions are larger than Na^+ ions. Also, although the sizes of Na^+ and Ca^+ are virtually identical, only half as many Ca^+ ions will be needed to blance the negative charge on the zeolite framework when they replace Na^+ ions, So the space down the centre of the pore when thes exchanges are mad will change accordingly (Mortimer and Taylor, 2002). Zeolite A have the potential continuous separation of gas vapor and non-aqueous mixture. Zeolite A are hydrophilic with excellemt separation properties for alcohol dehydration and solvent dewatering (Nogi, Naito and Yokoyama, 2012). Therefore, the concentration of ethanol solution was increased after adsorption with zeolite NaA modified with cations up to 95.3 - 99.8% (see Table 4.10).

The large poresize is faujasite (Zeolite X and Y) 7.4 Å (Čejka and Van Bekkum, 2005), the faujasite pore system is very open and three dimensional. It is constructed of sodalite cages connected by oxygen bridges through the six- membered - ring faces. This gives an array of nearly spherical cavities (1.14 nm diameter) each of which is accessed via four tetrahedrally orientated 0.74 nm ports. The overall pore structure, which is comparable to the carbon - carbon bonding structure in diamond. zeolite X with a large pore size 7.3 Å and a hight CEC, wich make this zeolite an interesting molecular sieve and cation exchange material (Cox et al., 2008). The concentration of ethanol solution was increased after adsorption with zeolite NaX modified with cations up to 95.7- 99.1% (see Table 4.11).

Modification zeolite NaA and zeolite NaX with Co^{2+} are much more capable to eliminate water compared to the other modified zeolites, 99.8 and 99.1%. A propensity of Co^{2+} to form four- and six-coordinate complexes an result in similar molecular structures of $CoCl_2$ complexes with some O-donor ligands. The two cobalt atoms are each coordinated to six oxygen atoms in an octahedral arrangement. One of the cobalt octahedra contains only oxygen atoms from six formate ions. The second cobalt ion is surrounded by four water molecules and an oxygen atom from each of two formate ions. The two different octahedra are bridged by one of the formate ions and by hydrogen bonds. This network extends in a three-dimensional polymeric manner throughout the crystal structure. Each of the four oxygen atoms in the two independent formate ions forms a hydrogen bond to water and is coordinated to a metal ion. It is found that the metal ions lie in the plane of the formate carboxyl group to which they are coordinated, while molecules to which the formate ion is hydrogen bonded lie more out of this plane (Kaufman, Afshar, Rossi, Zacharias and Glusker, 1993).

The actual pore size and the affinity between adsorbed molecules and the pore-wall depend on the type of cation and level of ion exchange (Oyama and Stagg-Williams, 2011).

Table 4.9 Concentration of ethanol solution before and after adsorption with analcime

    and cancrinite.

	Concentration of ethanol (% v/v)	
Initial concentration	**85.0%**	**95.0%**
Analcime	96.4	99.6
Cancrinite	94.9	99.3

Table 4.10 Concentration of ethanol solution before and after adsorption with zeolite

    NaA and cationic modified zeolite NaA.

Initial concentration	Concentration of ethanol (% v/v)	
	85.0%	**95.0%**
Zeolite NaA	88.2	98.0
NaA modified with K^+	87.5	95.9
NaA modified with Mg^{2+}	89.9	98.0
NaA modified with Ca^{2+}	88.0	98.3
NaA modified with Sr^{2+}	86.5	98.5
NaA modified with Co^{2+}	98.2	99.8
NaA modified with Ni^{2+}	88.6	95.3
NaA modified with Cu^{2+}	89.9	97.7
NaA modified with Zn^{2+}	93.1	97.5

Table 4.11 Concentration of ethanol solution before and after adsorption with zeolite

NaX and cationic modified zeolite NaX.

	Concentration of ethanol (% v/v)	
Initial concentration	**85.0%**	**95.0%**
Zeolite NaX	89.7	95.9
NaX modified with K^+	92.2	95.7
NaX modified with Mg^{2+}	89.0	96.2
NaX modified with Ca^{2+}	91.9	97.2
NaX modified with Sr^{2+}	89.1	96.7
NaX modified with Co^{2+}	98.2	99.1
NaX modified with Ni^{2+}	92.5	96.6
NaX modified with Cu^{2+}	91.7	97.1
NaX modified with Zn^{2+}	90.9	96.9

CHAPTER V

CONCLUSION

Adsorption is an alternative technology to purify ethanol. Therefore, in this work the elimination of water from ethanol solution using zeolite molecular sieves such as analcime, cancrinite, zeolite NaA, zeolite NaX and their modification with various cations.

The experrimental investigations on the sodium zeolites from kaolin and diatomite materials proved that these materials are a low cost silica - alumina material suitable for zeolite synthesis. The synthesis of analcime and cancrinite was carried out by using diatomite, diatomite treated with 6 M H_2SO_4 for elimination of aluminum and followed by calcinations at 900 °C and 1100 °C as silica sources. In the synthesis of analcime, 10% w/v of NaOH reacted with silica with the ratio of solid to liquid 1:10 (in g:mL) and $Al(OH)_3$ 0.2350 g. Then it was carried out in digestion bombs at autogenous pressures of the temperature at 140 °C with reaction time 120 hours. The synthesis of cancrinite was the same, but with the following condition employed: 20% w/v of NaOH: silica = 1:30 (in g:mL), reaction temperature of 180 °C and reaction time 72 hours. Analcime and cancrinite successfully synthesized from diatomite, the yields products synthesized were only single phase of analcime or cancrinite well and high crystallite.

The zeolitic products synthesized get the pure phase of zeolite NaA or zeolite NaX with good crystallinity.

These zeolite products obtained are very interesting because of their applications as molecular sieves for elimination of water from ethanol solution. The concentrations of ethanol after the adsorption with various adsorbents. The results showed that the concentration of ethanol solution was increased in all adsorbents. Analcime, cancrinite and modified zeolite NaA and zeolite NaX with Co^{2+} are much more capable to eliminate water compared to the others.
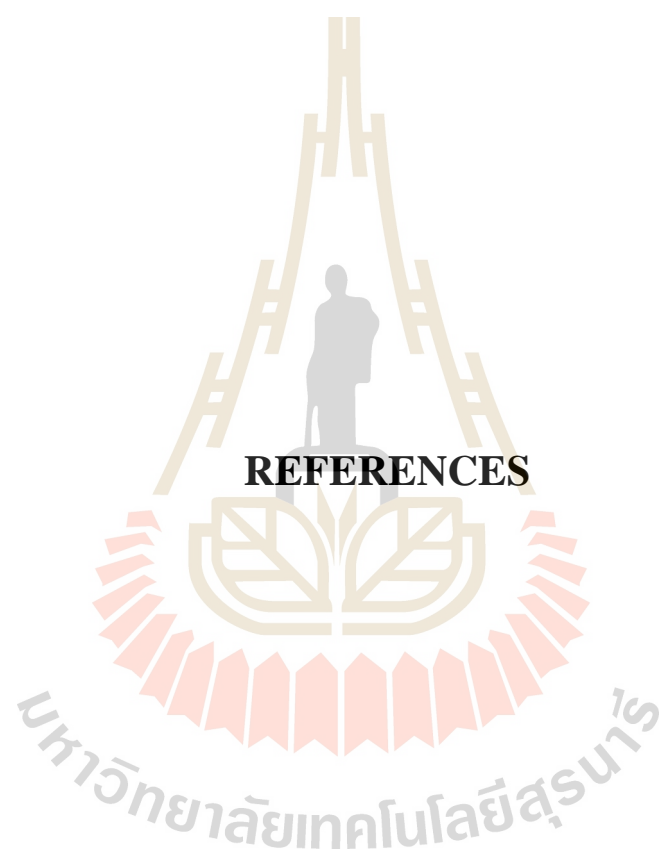
REFERENCES

REFERENCES

Akolekar, D., Chaffee, A., and Howe, R. F. (1997). The transformation of kaolin to low-silica X zeolite. **Zeolite**s. 19(5-6): 359-365.

Al-Asheh, S., Banat, F., and Al-Lagtah, N. (2004). Separation of Ethanol–Water Mixtures Using Molecular Sieves and Biobased Adsorbents. **Chemical Engineering Research and Design.** 82(7): 855-864.

Aouinti, L., and Belbachir, M. (2008). A maghnite-clay-H/ polymer membrane for separation of ethanol–water azeotrope. **Applied Clay Science.** 39(1-2): 78-85.

Atta, A. Y., Ajayi, O. A., and Adefila, S. S. (2007). Synthesis of Faujasite Zeolites from Kankara Kaolin Clay. **Journal of Applied Sciences Research.** 3(10): 1017- 1021.

Atta, A. Y., Jibril, B. Y., Aderemi, B. O., and Adefila, S. S. (2012). Preparation of analcime from local kaolin and rice husk ash. **Applied Clay Science.** 61(0): 8- 13.

Barrer, M. R. (1998). Molecular sieves:histoey and nomenclature molecular sieves. **Molecular sieves Principles of Synthesis and Identification.** 2: 1-28.

Beery, K. E., and Ladisch, M. R. (2001). Adsorption of Water from Liquid-Phase Ethanol–Water Mixtures at Room Temperature Using Starch-Based Adsorbents. **Industrial & Engineering Chemistry Research.** 40(9): 2112-2115.

Bekkum, H. V., Flanigen, E. M., and Jansen, J. C. (2001). **Introduction to zeolite science and practice, zeolite and molecular sieves.** 11-175.

Ben-Shebil, S. M. (1999). Effect of heat of adsorption on the adsorptive drying of solvents at equilibrium in a packed bed of zeolite. **Chemical Engineering Journal.** 74(3): 197-204.

Black, C., and Ditsler, D. E. (1974). Dehydration of Aqueous Ethanol Mixtures by Extractive Distillation Extractive and Azeotropic Distillation. **American Chemical Society.** 115: 1-15

Breck, D. W., and Flanigen, E. M. (1968). **Molecular sieve. Society of the chemical industry.** London, UK. p.47.

Breck, D. W. (1974). **Zeolite Molecular Sieves: structure chemistry and use.** Wiley. New York. 529-536.

Bui, S., Verykios, X., and Mutharasan, R. (1985). In situ removal of ethanol from fermentation broths. 1. Selective adsorption characteristics. **Industrial and Engineering Chemistry Process Design and Developmen**t. 24(4): 1209-1213.

Carmo, M. J., and Gubulin, J. C. (1997). Ethanol-water adsorption on commercial 3A zeolites: kinetic and thermodynamic data. **Brazilian Journal of Chemical Engineering.** 14: 1-10.

Carmo, M. J., and Gubulin, J. C. (2002). Ethanol-Water Separation in the PSA Process. **Adsorption.** 8(3): 235-248.

Carrado, K. A. (2003). **Handbook of Zeolite Science and Technology.** Marcel Dekker Incorporated.

Čejka, J., Corma, A., and Zones, S. (2010). **Zeolites and Catalysis: Synthesis, Reaction and Applications.** WILEY-VCH Verlag GmbH and Company.

Čejka, J., and Van Bekkum, H. (2005). **Zeolites and Ordered Mesoporous Materials: Progress and Prospects** : the 1st FEZA School on Zeolites, Prague, Czech Republic, August 20-21, 2005: Elsevier.

Chaisena, A., and Rangsriwatananon, K. (2005). Synthesis of sodium zeolites from natural and modified diatomite. **Materials Letters.** 59(12): 1474-1479.

Chandrasekhar, S., and Pramada, P. N. (1999). Investigation on the Synthesis of Zeolite NaX from Kerala Kaolin. **Journal of Porous Materials.** 6(4): 283-297.

Chatterjee, M., and Ganguli, D. (1982). Intermediate-stage transition metal ion exchange in a zeolite X. **Australian Journal of Chemistry.** 35(7): 1335-1340.

Cooley, R. S., and Schweitzer, P. A. (1996). **Handbook of Separation Techniques for Chemical Engineers.**

Cox, M., Nugteren, H., and Janssen-Jurkovičová, M. (2008). **Combustion Residues: Current, Novel and Renewable Applications.** John Wiley & Sons.

Ediz, N., Bentli, İ., and Tatar, İ. (2010). Improvement in filtration characteristics of diatomite by calcination. **International Journal of Mineral Processing.** 94(3–4): 129-134.

Ghobarkar, H. (2003). **The Reconstruction of Natural Zeolites.** Kluwer Academic Publishers.

Gilson, J. P. (2002). **Zeolites for Cleaner Technologies:** Imperial College Press.

Gualtieri, A., Norby, P., Artioli, G., and Hanson, J. (1997). Kinetics of formation of zeolite Na-A [LTA] from natural kaolinites. **Physics and Chemistry of Minerals.** 24(3): 191-199.

Handbook of zeolite science and technology. (2004). **Focus on Catalysts.** p. 8.

Hassaballah, A. A., and Hills, J. H. (1990). Drying of ethanol vapors by adsorption on corn meal. **Biotechnology and Bioengineering.** 35(6): 598-608.

Hu, X., and Xie, W. (2001). Fixed-bed adsorption and fluidized-bed Regeneration for breaking the azeotrope of ethanol and water. **Separation Science and Technology.** 36(1): 125-136.

Humphrey, J. L., and Keller, G. E. (1997). **Separation Process Technology.** Mcgraw-Hill.

Ismail, A. A., Mohamed, R. M., Ibrahim, I. A., Kini, G., and Koopman, B. (2010). Synthesis, optimization and characterization of zeolite A and its ion-exchange properties. **Colloids and Surfaces A: Physicochemical and Engineering Aspects.** 366(1–3): 80-87.

Joshi, U. D., Joshi, P. N., Tamhankar, S. S., Joshi, V. P., Idage, B. B., and Joshi, V. V. (2002). Influence of the size of extraframework monovalent cations in X-type zeolite on their thermal behavior. **Thermochimica Acta.** 387(2): 121-130.

Karge, H. G., and Weitkamp, J. (1998). **Molecular Sieves: Science and Technology.** Springer-Verlag.

Khaleghian-Moghadam, R., and Seyedeyn-Azad, F. (2009). A study on the thermal behavior of low silica X-type zeolite ion-exchanged with alkaline earth cations. **Microporous and Mesoporous Materials.** 120(3): 285-293.

King, R. B. (1994). **Encyclopedia of inorganic chemistry.** Wiley.

Ladisch, M. R., Voloch, M., Hong, J., Bienkowski, P., and Tsao,T. G. (1984). Cornmeal Adsorption for Dehydrating Ethanol Vapors. **Industrial and Engineering Chemistry Process Design and Development.** 23: 437-443

Lei, Z., Wang, H., Zhou, R., and Duan, Z. (2002). Influence of salt added to solvent on extractive distillation. **Chemical Engineering Journal.** 87(2): 149-156.

Mathewson, S. W. (1980). **The Manual for the Home and Farm Production of Alcohol Fuel.** Ten Speed Press.

Mortimer, M., Taylor, P., Chemistry, R. S. o., and University, O. (2002). **Chemical Kinetics and Mechanism.** Royal Society of Chemistry.

Namboodiri, V. V., and Vane, L. M. (2007). High permeability membranes for the dehydration of low water content ethanol by pervaporation. **Journal of Membrane Science.** 306(1–2): 209-215.

Navajas, A., Mallada, R., Téllez, C., Coronas, J., Menéndez, M., and Santamaría, J. (2002). Preparation of mordenite membranes for pervaporation of water-ethanol mixtures. **Desalination.** 148(1–3): 25-29.

Nogi, K., Naito, M., and Yokoyama, T. (2012). **Nanoparticle Technology Handbook.** Elsevier Science.

Oyama, S. T., and Stagg-Williams, S. M. (2011). **Inorganic, Polymeric and Composite Membranes: Structure, Function and Other Correlations.** Elsevier Science.

Pruksathorn, P., and Vitidsant, T. (2009). Production of pure ethanol from azeotropic solution by pressure swing adsorption. **Korean Journal of Chemical Engineering.** 26(4): 1106-1111.

Ríos, C. A., Williams, C. D., and Fullen, M. A. (2009). Nucleation and growth history of zeolite LTA synthesized from kaolinite by two different methods. **Applied Clay Science.** 42(3–4): 446-454.

Robson, H. E. (2001). **Verified Syntheses of Zeolitic Materials.** Elsevier.

Rocha, J., Klinowski, J., and Adams, J. M. (1991). Synthesis of zeolite Na-A from metakaolinite revisited. **Journal of the Chemical Society, Faraday Transactions.** 87(18): 3091-3097.

Sato, K., Aoki, K., Sugimoto, K., Izumi, K., Inoue, S., and Saito, J. (2008). Dehydrating performance of commercial LTA zeolite membranes and application to fuel grade bio-ethanol production by hybrid distillation/vapor permeation process. **Microporous and Mesoporous Materials.** 115(1–2); 184-188.

Sato, K., Sugimoto, K., Sekine, Y., Takada, M., Matsukata, M., and Nakane, T. (2007). Application of FAU-type zeolite membranes to vapor/gas separation under high pressure and high temperature up to 5MPa and 180 °C. **Microporous and Mesoporous Materials.** 101(1–2): 312-318.

Shi, J., Wang, J., Yu, G., and Chen, M. (1996). **Chemical Engineering Handbook.**

Sowerby, B., and Crittenden, B. D. (1988). An experimental comparison of type A molecular sieves for drying the ethanol-water azeotrope. **Gas Separation and amp; Purification.** 2(2): 77-83.

Stepto, R. F. T., and Szostak, R. (1997). **Molecular Sieves: Principles of Synthesis and Identification.** Blackie Academic and Professional

Szostak, R. (1992). **Handbook of Molecular Sieves: Van Nostrand Reinhold.** New York.

Szostak, R. (1998). **Molecular Sieves Principles of Synthesis and Identification.** Van Nostrand Reinhols: New York.

Teo, W. K., and Ruthven, D. M. (1986). Adsorption of water from aqueous ethanol using 3-.ANG. molecular sieves. **Industrial & Engineering Chemistry Process Design and Development.** 25(1): 17-21.

Thammavong, S. (2003). **Studies of synthesis, Kinetics and particle size of zeolite X from Narathiwat Kaoline.** M.Sc. Thesis, Suranaree University of Technology.

Wang, Y., Gong, C., Sun, J., Gao, H., Zheng, S., and Xu, S. (2010). Separation of ethanol/water azeotrope using compound starch-based adsorbents. **Bioresource Technology.** 101(15): 6170-6176.

Wongwiwattana, J. (2002). **Synthesis and kinetic study of zeolite Na-A from Thai Kaolin.** M.Sc. Thesis, Suranaree University of Technology.

Xie, W. (1999). **Preparation of Anhydrous Ethanol by Vapor Phase Adsorption Method.**

Xu, R. (2007). **Chemistry of Zeolites and Related Porous Materials.** Synthesis and
Structure: John Wiley and Sons (Asia).

Xu, R., Pang, W., Yu, J., Huo, Q., and Chen, J. (2010). **Structural Chemistry of
Microporous Materials Chemistry of Zeolites and Related Porous
Materials.** 19-116.

Yang, R. T. (1987). **Gas Separation by Adsorption Processes.** Imperial College
Press.

Żbik, M. S., Raftery, N. A., Smart, R. S. C., and Frost, R. L. (2010). Kaolinite platelet
orientation for XRD and AFM applications. **Applied Clay Science.** 50(3):
299-304.
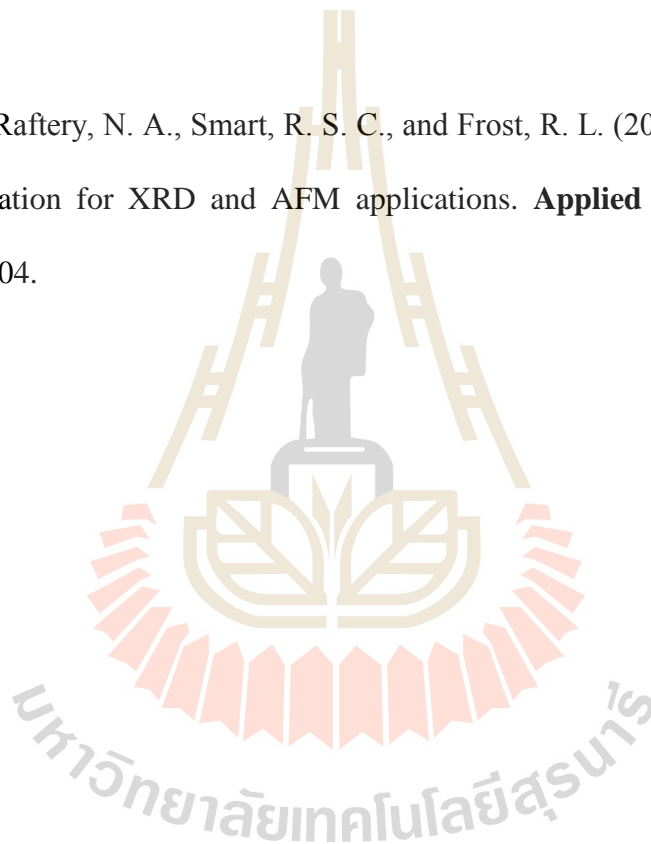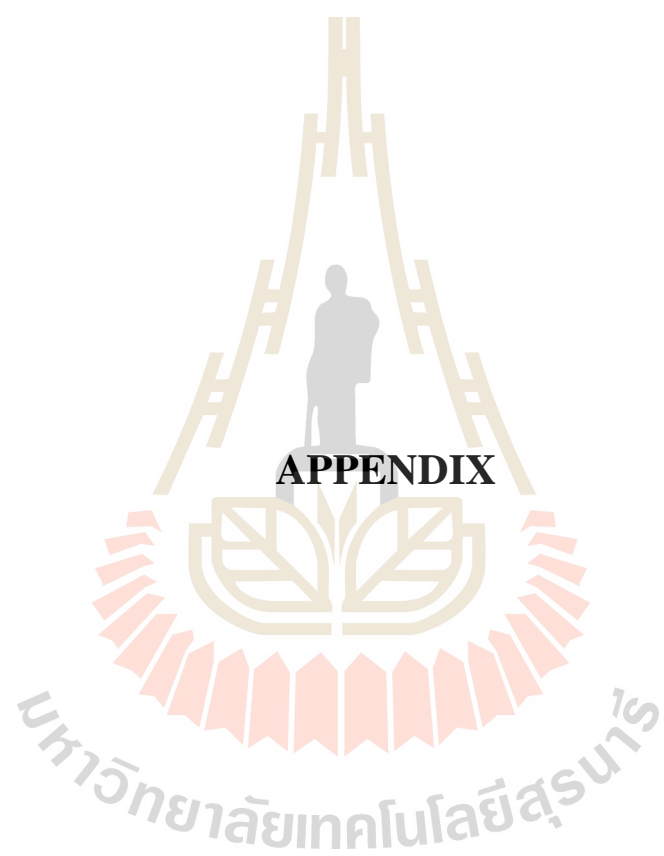
APPENDIX

APPENDIX

ANA Analcime

CHEMICAL COMPOSITION: $|Na_{16}(H_2O)_{16}|$ $[Si_{32}Al_{16}O_{96}]$
Cyclopean Islands, Greece

REFINED COMPOSITION: $|Na_{16}(H_2O)_{16}|$ $[Si_{32}Al_{16}O_{96}]$

CRYSTAL DATA: $Ia\overline{3}d$ (No. 230)
$a = 13.73$ Å $b = 13.73$ Å $c = 13.73$ Å
$\alpha = 90°$ $\beta = 90°$ $\gamma = 90°$
X-ray single crystal refinement, $R = 0.04$

REFERENCE: G. Ferraris, D. W. Jones and J. Yerkess,
$Z.$ $Kristallogr.$ **135** 240–252 (1972).

h	k	l	2θ	d	M	I_{rel}	h	k	l	2θ	d	M	I_{rel}	h	k	l	2θ	d	M	I_{rel}
2	1	1	15.81	5.605	24	60.2	5	2	1	35.82	2.507	48	11.9	4	4	4	45.78	1.982	8	0.4
2	2	0	18.28	4.854	12	14.1	4	4	0	37.04	2.427	12	7.7	5	4	3	46.78	1.942	48	0.7
3	2	1	24.25	3.669	48	5.4	6	1	1	40.50	2.227	24	2.8	6	4	0	47.77	1.904	24	14.9
4	0	0	25.96	3.433	6	100.0	5	3	2	40.50	2.227	48	5.5	5	5	2	48.74	1.868	24	0.2
3	3	2	30.54	2.927	24	51.3	6	2	0	41.60	2.171	24	1.0	6	3	3	48.74	1.868	24	6.9
4	2	2	31.93	2.803	24	5.5	5	4	1	42.68	2.119	48	0.9	7	2	1	48.74	1.868	48	2.3
4	3	1	33.27	2.693	48	14.8	6	3	1	44.77	2.024	48	1.3	6	4	2	49.69	1.835	48	0.4

Analcime   ANA
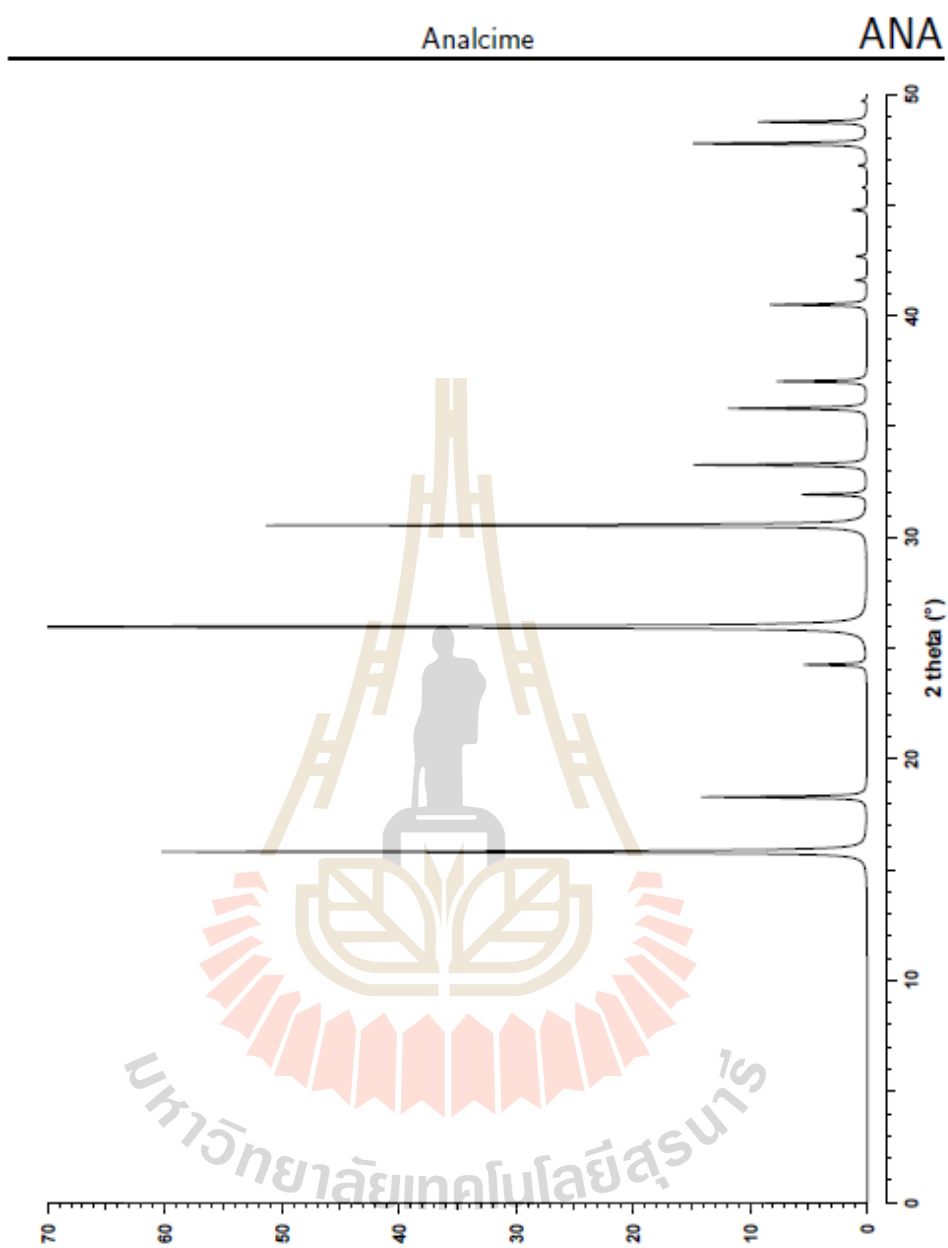
CAN

Cancrinite

CHEMICAL COMPOSITION: $|Na_7Ca_{0.9}(CO_3)_{1.4}(H_2O)_{2.1}|\ [Si_6Al_6O_{24}]$
Synthetic crystal.

REFINED COMPOSITION: $|Na_8(CO_3)_{1.2}(H_2O)_2|\ [Si_6Al_6O_{24}]$

CRYSTAL DATA: $P6_3$ (No. 173)
$a = 12.635$ Å $b = 12.635$ Å $c = 5.115$ Å
$\alpha = 90°$ $\beta = 90°$ $\gamma = 120°$
X-ray single crystal refinement, $R = 0.04$

REFERENCE: Y. I. Smolin, Y. F. Shepelev, I. K. Butikova and I. B. Kobyakov,
Kristallografiya **26** 63–66 (1981).

h	k	l	2θ	d	M	I_{rel}	h	k	l	2θ	d	M	I_{rel}	h	k	l	2θ	d	M	I_{rel}
1	0	0	8.08	10.942	6	3.9	2	2	1	33.34	2.688	12	0.1	2	1	2	41.51	2.175	12	1.9
1	1	0	14.02	6.317	6	59.5	3	1	1	34.36	2.610	12	10.2	1	4	1	41.75	2.164	12	6.7
2	0	0	16.20	5.471	6	3.7	1	3	1	34.36	2.610	12	19.8	4	1	1	41.75	2.164	12	4.4
1	0	1	19.15	4.634	12	100.0	0	0	2	35.09	2.557	2	42.0	3	3	0	42.95	2.106	6	21.6
1	2	0	21.49	4.136	6	0.6	3	2	0	35.77	2.510	6	1.3	3	0	2	43.20	2.094	12	13.6
2	1	0	21.49	4.136	6	6.1	2	3	0	35.77	2.510	6	1.7	2	4	0	43.78	2.068	6	0.2
1	1	1	22.36	3.975	12	1.0	1	0	2	36.06	2.490	12	1.2	5	0	1	45.06	2.012	12	4.9
2	0	1	23.81	3.736	12	2.7	4	0	1	37.27	2.412	12	34.0	2	2	2	45.64	1.988	12	0.5
3	0	0	24.40	3.647	6	55.1	1	4	0	37.67	2.388	6	3.4	5	1	0	46.19	1.965	6	0.5
1	2	1	27.74	3.216	12	56.9	4	1	0	37.67	2.388	6	0.7	3	1	2	46.43	1.956	12	0.4
2	1	1	27.74	3.216	12	61.4	1	1	2	37.96	2.371	12	1.1	1	3	2	46.43	1.956	12	0.5
2	2	0	28.25	3.159	6	0.3	2	0	2	38.87	2.317	12	2.6	2	4	1	47.42	1.917	12	1.3
3	1	0	29.43	3.035	6	0.9	2	3	1	40.01	2.254	12	10.4	4	2	1	47.42	1.917	12	1.1
1	3	0	29.43	3.035	6	3.2	3	2	1	40.01	2.254	12	10.4	4	0	2	48.74	1.868	12	13.1
3	0	1	30.09	2.970	12	4.3	5	0	0	41.25	2.188	6	1.7	1	5	1	49.70	1.835	12	0.5
4	0	0	32.74	2.736	6	42.6	1	2	2	41.51	2.175	12	1.5	5	1	1	49.70	1.835	12	0.3

Cancrinite   CAN
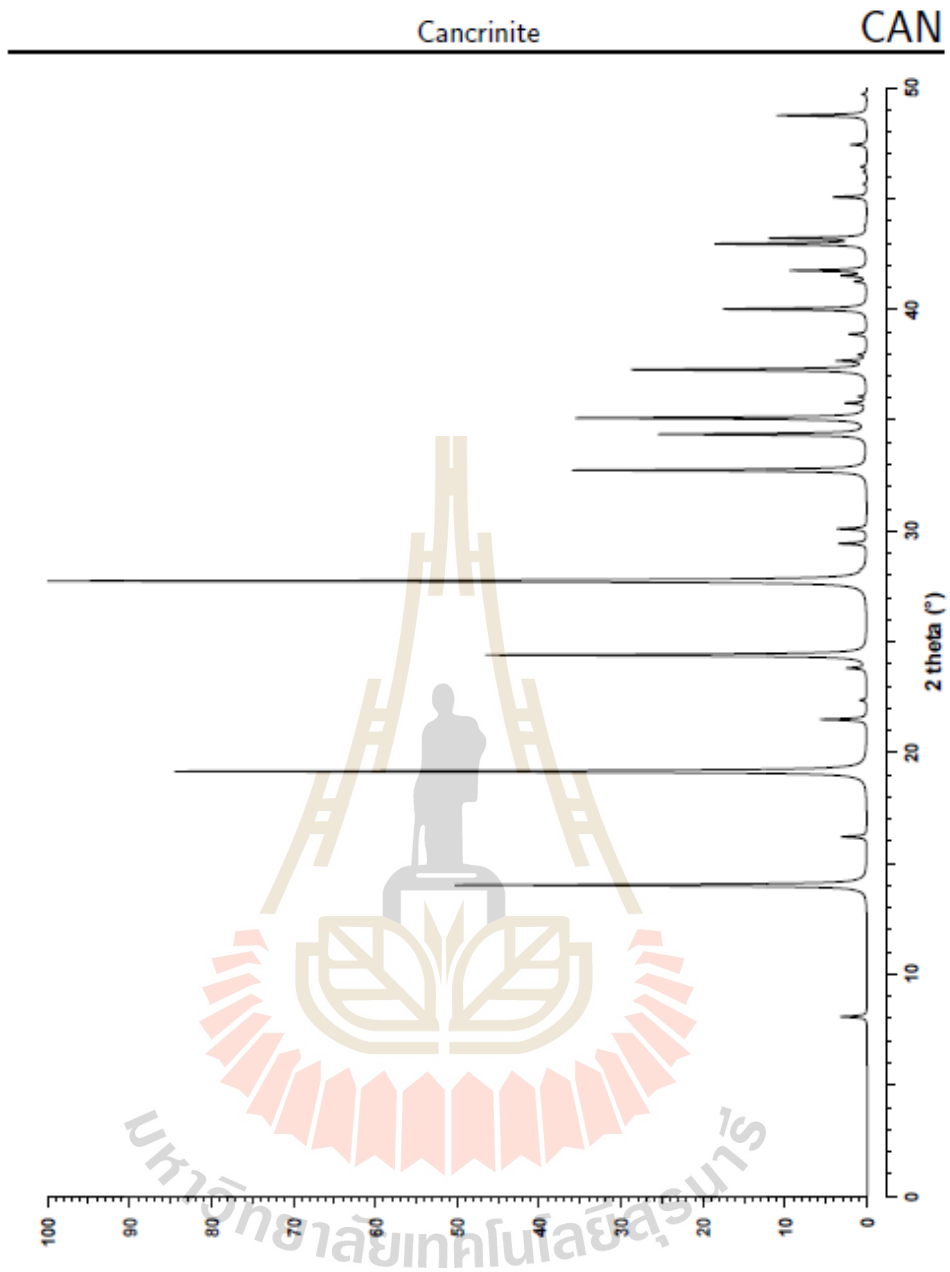
FAU

Na-X, Hydrated

CHEMICAL COMPOSITION: $|Na_{88}(H_2O)_{220}|\ [Si_{104}Al_{88}O_{384}]$

REFINED COMPOSITION: $|Na_{40.32}(H_2O)_{171.84}|\ [Si_{103.68}Al_{88.32}O_{384}]$

CRYSTAL DATA: $Fd\overline{3}$ (No. 203) origin at centre ($\overline{3}$)
$a = 25.028$ Å $b = 25.028$ Å $c = 25.028$ Å
$\alpha = 90°$ $\beta = 90°$ $\gamma = 90°$
X-ray single crystal refinement, $R = 0.09$

REFERENCE: D. H. Olson,
J. Phys. Chem. **74** 2758–2764 (1970).

h	k	l	2θ	d	M	I_{rel}	h	k	l	2θ	d	M	I_{rel}	h	k	l	2θ	d	M	I_{rel}
1	1	1	6.12	14.450	8	100.0	6	6	0	30.30	2.950	12	1.0	11	1	1	39.95	2.257	24	0.2
2	2	0	10.00	8.849	12	10.4	8	2	2	30.30	2.950	24	1.7	7	7	5	39.95	2.257	24	0.3
3	1	1	11.73	7.546	24	3.8	7	1	5	30.94	2.890	24	0.4	8	8	0	40.79	2.212	12	1.1
2	2	2	12.25	7.225	8	0.2	7	5	1	30.94	2.890	24	0.4	11	1	3	41.29	2.187	24	0.3
3	3	1	15.43	5.742	24	6.5	5	5	5	30.94	2.890	8	5.7	11	3	1	41.29	2.187	24	0.3
4	2	2	17.36	5.109	24	0.1	6	6	2	31.15	2.871	24	0.2	9	5	5	41.29	2.187	24	0.1
3	3	3	18.42	4.817	8	0.3	8	0	4	31.98	2.798	12	1.6	9	7	1	41.29	2.187	24	0.2
5	1	1	18.42	4.817	24	1.3	8	4	0	31.98	2.798	12	1.8	9	1	7	41.29	2.187	24	0.2
4	4	0	20.07	4.424	12	2.0	7	3	5	32.59	2.747	24	0.1	8	8	2	41.45	2.178	24	0.1
5	3	1	21.00	4.231	24	0.6	9	1	1	32.59	2.747	24	0.1	11	3	3	42.59	2.123	24	0.6
6	2	0	22.47	3.957	12	1.1	7	5	3	32.59	2.747	24	0.4	8	8	4	43.38	2.086	24	0.3
6	0	2	22.47	3.957	12	0.2	8	4	2	32.80	2.731	24	0.1	9	9	1	46.31	1.960	24	0.3
5	3	3	23.31	3.817	24	6.2	8	2	4	32.80	2.731	24	0.1	12	4	2	46.46	1.954	24	0.3
6	2	2	23.58	3.773	24	0.5	6	6	4	33.59	2.668	24	3.4	12	2	4	46.46	1.954	24	0.2
4	4	4	24.64	3.612	8	0.2	9	3	1	34.17	2.624	24	0.5	10	8	2	47.06	1.931	24	0.4
5	5	1	25.41	3.505	24	0.2	9	1	3	34.17	2.624	24	0.6	10	2	8	47.06	1.931	24	0.2
6	2	4	26.65	3.345	24	2.4	8	4	4	35.13	2.554	24	0.5	12	4	4	48.24	1.887	24	0.2
6	4	2	26.65	3.345	24	3.2	8	2	6	36.61	2.454	24	0.1	9	7	7	48.67	1.871	24	0.2
7	3	1	27.37	3.258	24	0.1	10	2	2	37.34	2.408	24	0.2	13	3	3	49.82	1.830	24	0.1
7	3	3	29.21	3.058	24	1.2	6	6	6	37.34	2.408	8	1.2	9	9	5	49.82	1.830	24	0.2

Na-X, Hydrated   FAU
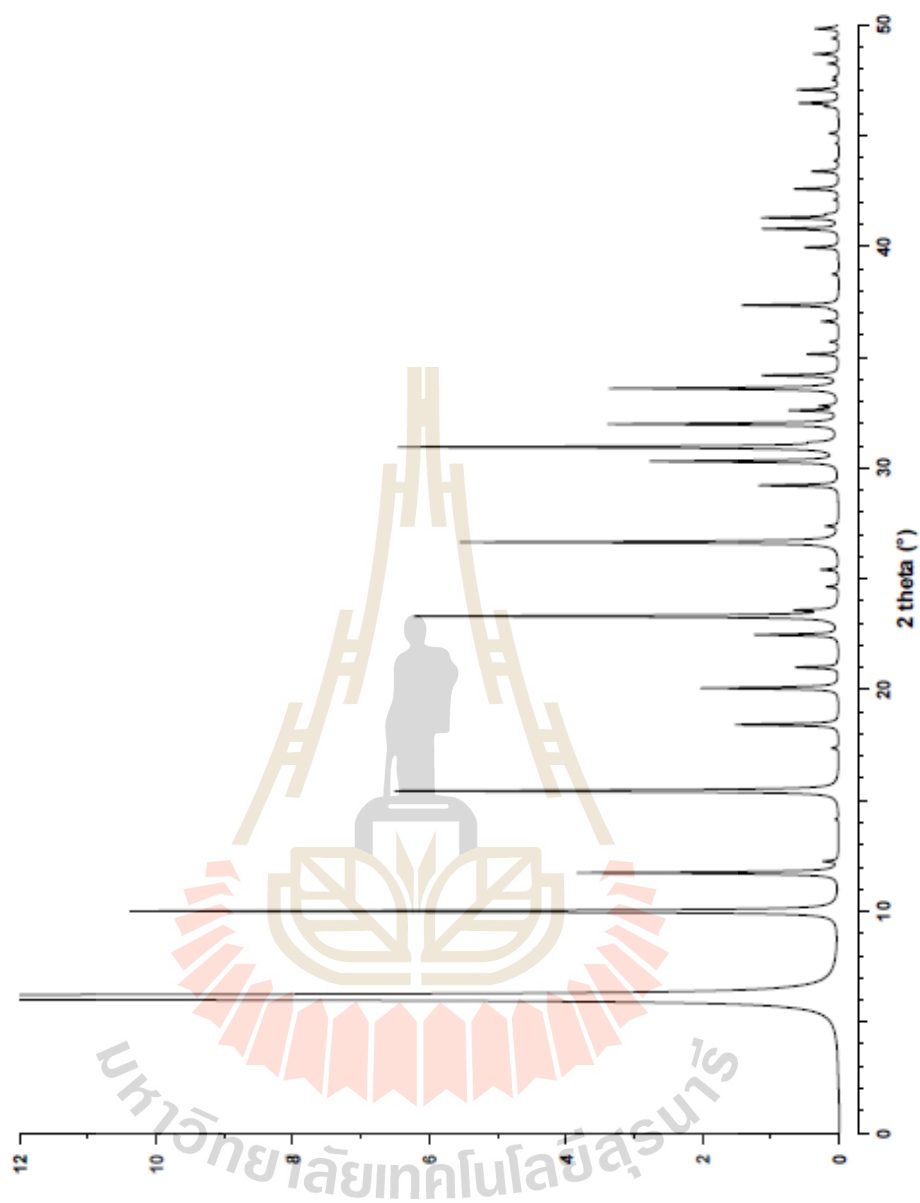
LTA
Linde Type A, Hydrated

CHEMICAL COMPOSITION: $|Na_{96}(H_2O)_{216}|\,[Si_{96}Al_{96}O_{384}]$

REFINED COMPOSITION: $|Na_{64}(H_2O)_{326.71}|\,[Si_{96}Al_{96}O_{384}]$

CRYSTAL DATA: $Fm\bar{3}c$ (No. 226)
$a = 24.61\ \text{Å}$ $b = 24.61\ \text{Å}$ $c = 24.61\ \text{Å}$
$\alpha = 90°$ $\beta = 90°$ $\gamma = 90°$
X-ray single crystal refinement, $R_w = 0.04$

REFERENCE: V. Gramlich and W. M. Meier,
*Z. Kristallogr.* **133** 134–149 (1971).

h	k	l	2θ	d	M	I_{rel}	h	k	l	2θ	d	M	I_{rel}	h	k	l	2θ	d	M	I_{rel}
2	0	0	7.18	12.305	6	100.0	8	2	2	30.83	2.900	24	5.4	8	6	6	42.85	2.110	24	2.3
2	2	0	10.17	8.701	12	51.3	6	6	0	30.83	2.900	12	2.3	10	6	0	42.85	2.110	24	1.2
2	2	2	12.46	7.104	8	31.8	6	6	2	31.70	2.823	24	0.2	10	6	2	43.51	2.080	48	1.8
4	0	0	14.40	6.153	6	0.5	8	4	0	32.54	2.751	24	9.3	8	8	4	44.16	2.051	24	0.9
4	2	0	16.11	5.503	24	20.3	8	4	2	33.37	2.685	48	3.0	12	0	0	44.16	2.051	6	7.8
4	2	2	17.65	5.023	24	2.4	6	6	4	34.18	2.623	24	27.1	12	2	0	44.80	2.023	24	0.5
4	4	0	20.41	4.350	12	3.6	9	3	1	34.77	2.580	48	0.1	12	2	2	45.44	1.996	24	0.1
5	3	1	21.36	4.160	48	2.1	8	4	4	35.75	2.512	24	4.7	12	4	0	46.69	1.946	24	0.2
6	0	0	21.67	4.102	6	10.6	10	0	0	36.51	2.461	6	4.1	10	8	0	47.30	1.922	24	2.3
4	4	2	21.67	4.102	24	22.8	8	6	0	36.51	2.461	24	0.4	8	8	6	47.30	1.922	24	4.2
6	2	0	22.85	3.891	24	1.2	10	2	0	37.26	2.413	24	0.1	12	4	2	47.30	1.922	48	0.3
6	2	2	23.99	3.710	24	44.3	10	2	2	38.00	2.368	24	1.6	10	8	2	47.91	1.899	48	5.1
4	4	4	25.07	3.552	8	0.7	6	6	6	38.00	2.368	8	1.4	10	6	6	48.51	1.876	24	0.3
6	4	0	26.11	3.413	24	10.1	8	6	4	39.43	2.285	48	1.0	12	4	4	49.11	1.855	24	0.9
6	4	2	27.11	3.289	48	41.0	10	4	0	39.43	2.285	24	0.3	10	8	4	49.70	1.834	48	1.8
8	0	0	29.03	3.076	6	0.4	10	4	2	40.14	2.247	48	2.2	12	6	0	49.70	1.834	24	0.9
6	4	4	29.94	2.984	24	19.7	8	8	0	41.51	2.175	12	4.3							
8	2	0	29.94	2.984	24	19.9	10	4	4	42.19	2.142	24	3.4							

Linde Type A, Hydrated LTA
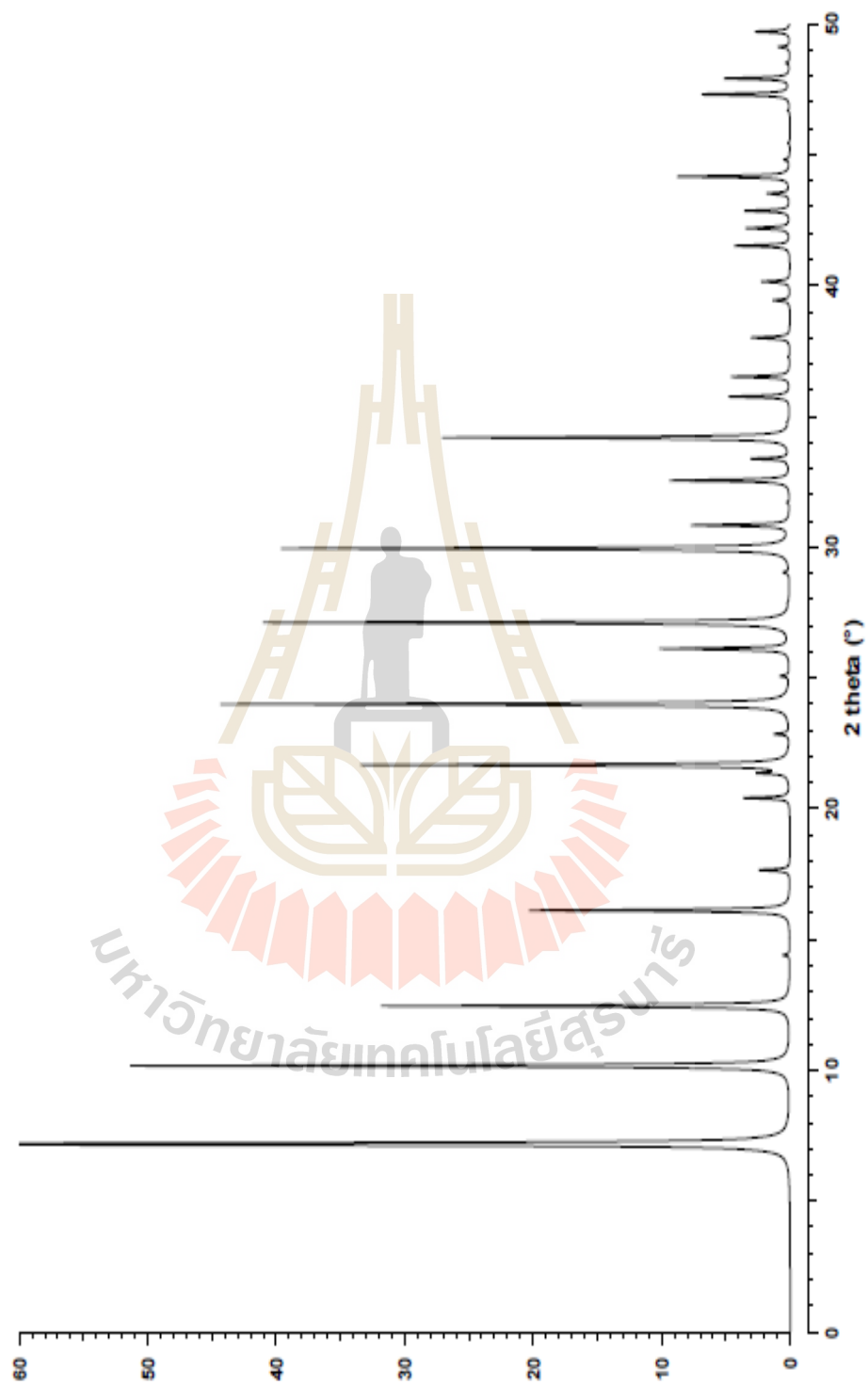
CURRICULUM VITAE

NAME: Kongla Muenpoowonk **DATE OF BIRTH:** 24 February, 1983

PLACE OF BIRTH: Ubon Ratchathani, Thailand **CITIZENSHIP:** Thai

EDUCATIONAL BACKGROUND:

2002 - 2005   Bachelor of Science (Chemistry), Ubon Ratchathani Rajbhat University, Ubon Ratchathani, Thailand

EXPERIENCE:

2006 - present   Teaching assistant at Suranaree University of Technology, Nakhon Ratchasima, Thailand

PRESENTATION:

1. "EFFECT OF STARTING MATERIAL ON THE SYNTHESIS OF SODIUM ZEOLITES", Pure and Applied Chemistry International Conference 2009, Ubonratchathani University, Thailand. January 21 – 23, 2010.

2. "COMPARED SILICA SOURCES ON THE SYNTHESIS OF ANALCIME AND CANCRINITE", The 3th Science Research Conference, Naresuan University**,** Thailand. March 14 – 15, 2011.

3. "ELIMINATION OF WATER FROM ETHANOL SOLUTION BY ZEOLITES", Pure and Applied Chemistry International Conference 2012, Chang Mai University, Thailand. January 11 – 13, 2012.